UNIVERSITY OF HELSINKI REPORT SERIES IN PHYSICS

HU-P-D243

ORGAN DOSE DETERMINATION IN X-RAY IMAGING

Anna Kelaranta

Department of Physics

Faculty of Science

University of Helsinki

Helsinki, Finland

HUS Medical Imaging Center

Helsinki University Hospital

Helsinki, Finland

ACADEMIC DISSERTATION

To be presented, with the permission of the Faculty of Science of the University of Helsinki, for public examination in Auditorium A110 of Chemicum, A. I. Virtasen aukio 1, Helsinki, on October 7th 2016 at 12 o´clock noon.

Helsinki, 2016

Supervising professor:

Professor Sauli Savolainen, Ph.D.
Division of Materials Physics
Department of Physics
University of Helsinki, Finland

HUS Medical Imaging Center
University of Helsinki and Helsinki University Hospital, Finland

Supervisors:

Docent Paula Toroi, Ph.D.
Section of Dosimetry and
Medical Radiation Physics
Department of Nuclear Sciences and
Applications
International Atomic Energy Agency,
Austria

Radiation Metrology Laboratory and
Occupational Exposure (previous position)
Department of Radiation Practices Regulation
Radiation and Nuclear Safety Authority, Finland

Docent Antti Kosunen, Ph.D.
Radiation Metrology Laboratory and
Occupational Exposure
Department of Radiation Practices
Regulation
Radiation and Nuclear Safety Authority,
Finland

Reviewers:

Docent Jari Heikkinen, Ph.D.
Department of Medical Physics
The Social and Health Care Joint Authority
of South Savo, Mikkeli Central Hospital,
Finland

Docent Juha Nikkinen, Ph.D.
Department of Oncology and Radiotherapy
Oulu University Hospital, Finland

Opponent:

Professor Miika Nieminen, Ph.D.
Department of Radiology
University of Oulu and Oulu University Hospital, Finland

ISSN 0356-0961

ISBN 978-951-51-2224-7 (printed version)

ISBN 978-951-51-2225-4 (pdf version)

Unigrafia Oy

Helsinki, 2016

A. Kelaranta: Organ dose determination in X-ray imaging, University of Helsinki, 2016, 51 pages + appendices. University of Helsinki, Report Series in Physics, HU-P-D243

Keywords: organ dose, fetal dose, phantom, conversion coefficient, patient size, radiation quality, lead shielding

Classification (INSPEC): A8760M, A8760P, A8770E, B7510P, B7530B

Abstract

Organ dose is the absorbed radiation energy from ionizing radiation to an organ, divided by the organ mass. Organ doses of a patient cannot be measured directly in the patient, but their determination requires dose measurements in anthropomorphic patient models i.e. phantoms or Monte Carlo simulations. Monte Carlo simulations can be performed for example by using computational phantoms or patient's computed tomography (CT) images. Organ doses can be estimated based on measurable dose quantities, such as air kerma, kerma-area product and volume-weighted CT dose index, by using suitable conversion coefficients. Conversion coefficient is the organ dose divided by the measured or calculated examination-specific dose quantity.

According to the current knowledge, the probability of radiation induced stochastic effects, which include cancer risk and risk of hereditary effects, increases linearly as a function of the radiation dose. The organ dose is a better quantity for estimating the patient specific risk than the effective dose, which is meant to be used only for populations, and it does not consider patient age or gender. Moreover, the tissue weighting factors that are used in the effective dose calculation are based on whole body irradiations, but in X-ray examinations only a part of the patient is exposed to radiation.

The phantoms used in medical dosimetry are either computational or physical, and computational phantoms are further divided into mathematical and voxel phantoms. Phantoms from simplified to as realistic as possible have been developed to simulate different targets, but the organ doses determined based on them can differ largely from the real organ doses of the patient. There are also standard and reference phantoms in use, which offer a dose estimate to a so called average patient. Due to the considerable variation within patient anatomies, the real dose might differ from the dose to a standard or reference phantom.

The aim of this thesis was to determine organ doses based on dose measurements and Monte Carlo simulations in four X-ray imaging modalities, including general radiography, CT, mammography and dental radiography. The effect of the patient and phantom thickness and radiation quality on the organ doses in a projection X-ray examination of the thorax was studied via Monte Carlo simulations by using both mathematical phantoms and patient CT images. The effect of the breast thickness on the mean glandular doses (MGDs) was determined based on measurements with phantoms of different thicknesses and collected diagnostic and screening data from patient examinations, and the radiation qualities used in patient and phantom exposures were studied. For fetal dose estimation, fetal dose conversion coefficients were determined based on phantom measurements in CT and dental radiography examinations. Additionally, the effect of lead shields on fetal and breast doses was determined in dental examinations.

The difference between Monte Carlo simulated organ doses in patients and mathematical phantoms was large, for the examined organs up to 55% in projection imaging. In mammographic examinations, the difference between MGDs calculated based on collected patient data and phantom measurements was up to 30%. In mammography, patient dose data cannot be replaced by phantom measurements. The properties and limitations of the phantoms must be known when they are used.

The estimation of the fetal dose based on conversion coefficients requires understanding about the cases where conversion coefficients are applicable. When used correctly, they provide a method for simple dose estimation, where the application specific dose quantity can be taken into account. The conversion coefficients determined in this thesis can be used to estimate the fetal dose in CT examination based on the volume-weighted CT dose index ($CTDI_{vol}$), and in dental examinations based on the dose-area product (DAP).

In projection imaging, the lung and breast doses decreased as the patient's anterior-posterior thickness increased, but in mammography, the MGDs increased as the compressed breast thickness increased. In CT examinations, the fetal dose remained almost constant in examination where the fetus was totally within the primary radiation beam. When the fetus was outside of the primary beam, the fetal dose increased exponentially with the decreasing distance of the fetus from the scan range. As a function of the half value layer (HVL), the conversion coefficients in the studied projection imaging examination were more convergent than as a function of the tube voltage. The HVL alone describes better the radiation quality than the tube voltage alone, which requires also the definition of the total filtration. In mammography, it is possible to irradiate a phantom and a patient with the same equivalent thickness with different radiation qualities when automatic exposure control is used.

Despite the relatively large shielding effect achieved with lead shielding in dental imaging, the fetal dose without lead shielding and the related exposure-induced increase in the risk of childhood cancer death are minimal (less than 10 μGy and 10^{-5} %), so there is no need for abdominal shielding. The exposure-induced increase in the risk of breast cancer death is of the same order of magnitude as the increase in the risk of childhood cancer death, so also breast shielding was considered irrelevant. Most important is that a clinically justified dental radiographic examination must never be avoided or postponed due to a pregnancy.

A. Kelaranta: Elinannosten määrittäminen röntgentutkimuksissa, Helsingin Yliopisto, 2016, 51 sivua + liitteet. University of Helsinki, Report Series in Physics, HU-P-D243

Avainsanat: elinannos, sikiöannos, fantomi, konversiokerroin, potilaan koko, säteilylaatu, lyijysuoja

Luokitus (INSPEC): A8760M, A8760P, A8770E, B7510P, B7530B

Tiivistelmä

Elinannoksella tarkoitetaan elimeen ionisoivasta säteilystä absorboitunutta säteilyenergiaa jaettuna elimen massalla. Potilaan elinannoksia ei voi mitata suoraan potilaassa, vaan niiden määrittämiseen on käytettävä annosmittauksia ihmistä jäljittelevissä potilasvastineissa eli fantomeissa tai Monte Carlo simulaatioita. Monte Carlo simulaatioita voidaan tehdä käyttäen esimerkiksi laskennallisia fantomeita tai potilaan tietokonetomografiakuvia (TT-kuvia). Elinannoksia voidaan arvioida mitattavissa olevien annossuureiden, kuten ilmakerman, kerman ja pinta-alan tulon ja TT:n tilavuusannosindeksin, perusteella käyttäen sopivia konversiokertoimia. Konversiokertoimella tarkoitetaan elinannoksen ja mitatun tai lasketun tutkimuskohtaisen annossuureen suhdetta.

Nykykäsityksen mukaan säteilyn aiheuttamien satunnaisten vaikutusten todennäköisyys, joihin kuuluvat syöpäriski ja perinnöllisten vaikutusten riski, kasvaa lineaarisesti säteilyannoksen kasvaessa. Elinannos on parempi suure potilaskohtaisen riskin arviointiin kuin efektiivinen annos, joka on tarkoitettu käytettäväksi ainoastaan väestötasolla, eikä se huomioi potilaan ikää tai sukupuolta. Lisäksi efektiivisen annoksen laskennassa käytettävät kudosten painotuskertoimet perustuvat kokokehosäteilytyksiin, mutta röntgentutkimuksissa vain osa potilaan kehosta altistuu säteilylle.

Lääketieteellisessä dosimetriassa käytetyt fantomit ovat joko laskennallisia tai fysikaalisia, ja laskennalliset fantomit jaetaan edelleen matemaattisiin ja vokselifantomeihin. Fantomeita yksinkertaistetuista mahdollisimman realistisiin on kehitetty simuloimaan erilaisia kohteita, mutta niiden avulla määritetyt elinannokset voivat poiketa suurestikin potilaan todellisista elinannoksista. Käytössä on myös standardi- ja referenssifantomeita, joilla saadaan annosarvio niin sanotulle keskimääräiselle potilaalle. Koska potilaiden ominaisuudet vaihtelevat huomattavasti, saattaa todellinen annos poiketa standardi- tai referenssifantomin annoksesta.

Tämän työn tarkoituksena oli määrittää elinannoksia annosmittausten ja Monte Carlo simulaatioiden perusteella neljässä röntgenkuvausmodeliteetissa, mukaan lukien natiiviröntgentutkimukset, TT-tutkimukset, mammografiatutkimukset ja hammasröntgentutkimukset. Potilaan ja fantomin paksuuden ja säteilylaadun vaikutusta elinannoksiin rintakehän projektiotutkimuksessa selvitettiin Monte Carlo simulointien avulla käyttäen sekä matemaattisia fantomeita että potilaiden TT-kuvia. Rinnan paksuuden vaikutus keskimääräisiin rauhaskudosannoksiin mammografiassa määritettiin käyttäen mittauksissa eri paksuisia rintafantomeita sekä kerättyä diagnostista ja seulontamammografiadataa potilastutkimuksista, sekä tarkasteltiin potilas-ja fantomisäteilytyksissä käytettyjä säteilylaatuja. Sikiön annosarviointia varten määritettiin fantomimittausten avulla sikiön annoksen konversiokertoimia TT- ja

hammasröntgentutkimuksille. Lisäksi määritettiin lyijysuojien vaikutus sikiön ja rintojen annoksiin hammasröntgentutkimuksissa.

Eron potilaiden ja matemaattisen fantomin Monte Carlo simuloitujen elinannosten välillä todettiin olevan suuri, tarkasteltujen elinten osalta enimmillään 55% projektiotutkimuksissa. Mammografiatutkimuksissa ero kerätyn potilasdatan ja fantomien annosmittausten perusteella laskettujen keskimääräisten rauhaskudosannosten välillä oli enimmillään 30%. Mammografiassa fantomimittaukset eivät voi korvata potilasannosmäärityksiä. Fantomeiden ominaisuudet ja rajoitukset on tiedettävä niitä käytettäessä.

Sikiön annoksen arviointi konversiokertoimien avulla vaatii ymmärrystä siitä, mihin tilanteisiin konversiokertoimet soveltuvat. Oikein käytettynä ne tarjoavat menetelmän yksinkertaiseen annosarviointiin, jossa tutkimuskohtainen mitattavissa oleva annossuure voidaan ottaa huomioon. Tässä työssä määritettyjen konversiokerrointen avulla voidaan arvioida sikiön annosta TT-tutkimuksissa TT:n tilavuusannosindeksin avulla ja hammasröntgentutkimuksissa annoksen ja pinta-alan tulon avulla.

Projektiokuvauksessa potilaan anterior-posterior paksuuden kasvaessa keuhkojen ja rintojen annokset pienenivät, mutta mammografiassa keskimääräinen rauhaskudosannos kasvoi puristetun rinnan paksuuden kasvaessa. TT-tutkimuksissa sikiön annos pysyi eri raskausvaiheissa automaattisen putkivirran modulaation takia lähes vakiona sellaisissa tutkimuksissa, joissa sikiö oli kokonaan primäärisäteilykeilassa. Kun sikiö oli primäärisäteilykeilan ulkopuolella, sikiön annos kasvoi eksponentiaalisesti kun sikiön etäisyys kuvausalueen reunaan pieneni. Puoliintumispaksuuden (HVL) funktiona konversiokertoimet tarkastellussa projektiotutkimuksessa olivat yhtenäisemmät kuin putkijännitteen funktiona. Pelkkä HVL kuvaa siis paremmin säteilylaatua kuin pelkkä putkijännite, joka vaatii myös kokonaissuodatuksen määrittelyn. Mammografiassa on mahdollista automaattista säteilytysohjausta käytettäessä säteilyttää ekvivalenttipaksuudeltaan toisiaan vastaavat fantomi ja potilas eri säteilylaadulla.

Huolimatta lyijysuojauksella saavutetusta suhteellisesti suuresta annossäästöstä, sikiön annos ilman lyijysuojaa ja siihen liittyvä säteilystä aiheutuva lisäriski lapsuusiän syöpäkuolemalle ovat minimaalisia (alle 10 μGy ja 10^{-5} %), joten tarvetta vatsan alueen suojaukselle hammasröntgentutkimuksissa ei ole. Säteilystä aiheutuva lisäriski rintasyöpäkuolemalle on samaa suuruusluokkaa kuin lisäriski lapsuusiän syöpäkuolemalle, joten myöskään rintojen suojaus ei ole tarpeen. Tärkeintä on, että kliinisesti oikeutettua hammasröntgentutkimusta ei pidä koskaan välttää tai lykätä myöhemmäksi raskauden takia.

Preface

The work presented in this thesis was carried out during the years 2012 and 2016 at the Radiation and Nuclear Safety Authority (STUK) and the HUS Medical Imaging Center, Helsinki University Hospital. My research work during these years has been partly supported by State Subsidies for University Hospitals and a Ph.D. grant from The Finnish Cultural Foundation, of which I am eternally grateful. My Ph.D. studies took place at the Department of Physics at the University of Helsinki. I want to thank the director of the Radiation Practices Regulation Department of STUK, Eero Kettunen and the Managing and Deputy Managing Directors of the HUS Medical Imaging Center, Jyrki Putkonen and Pekka Tervahartiala for the opportunity to work with my research topics. I also owe my gratitude to the previous and current heads of the Department of Physics, Professor Juhani Keinonen and Professor Hannu Koskinen for supporting my Ph.D. studies at the University of Helsinki in the doctoral program in Materials Research and Nanosciences (MATRENA). I also want to thank the Radiological Society of Finland for the grant to finish my Ph.D. thesis.

I am most grateful to my supervisors, Docent Paula Toroi and Docent Antti Kosunen for their support and guidance through this project. Paula's passion for research has inspired me and our countless conversations about research and other topics have been an essential part for me in growing into the world of research. I'm also very grateful to Professor Sauli Savolainen, Chief Physicist of the HUS Medical Imaging Center, for his encouragement and advices for this Ph.D. project and also for the possibility to work as an expertizing physicist at the hospital.

I express my gratitude the official reviewers of this thesis, Docent Jari Heikkinen and Docent Juha Nikkinen, for their valuable comments and suggestions. I thank Professor Miika Nieminen for accepting the invitation to be the official opponent at my dissertation.

Research cannot be done alone. I want to warmly thank my co-authors, Docent Paula Toroi, Professor emeritus Peter Vock, Ph.D. Touko Kaasalainen, M.D. Raija Seuri, Docent Mika Kortesniemi, Ph.D. Marjut Timonen, Ph.D. Soile Komssi and D.M.D. Marja Ekholm. I feel privileged because I have had the possibility to work with all of them. I also want to thank all my previous and current colleagues and workmates in Kotka, Helsinki and Espoo for their help, advices and company during the years.

I want to thank Professor emeritus Juha Hernesniemi and his neurologic surgery team for *craniotomia occipitalis – suboccipitalis et exstirpatio pineolomatis*, which changed the direction of my life in 2007 and led me to the world of medical physics.

I wish my warm gratitude to my parents, Päivi Kelaranta and Arvo Juutilainen, and to my brother, cousins and friends. Finally, I want to thank my beloved fiancé, Patrik Ahvenainen, for his enormous support, patience and love during the years.

LIST OF ORIGINAL PUBLICATIONS

I **Kelaranta A**, Toroi P, Vock P. Organ dose conversion factors in thorax X-ray examinations: the effect of patient thickness and radiation quality. Submitted in revised form to Physica Medica: European Journal of Medical Physics 3.9.2016.

II **Kelaranta A**, Kaasalainen T, Seuri R, Toroi P, Kortesniemi M, 2015. Fetal radiation dose in computed tomography. Radiation Protection Dosimetry, 165 (1-4), pp. 226-230.

III **Kelaranta A**, Toroi P, Timonen M, Komssi S, Kortesniemi M, 2014. Conformance of mean glandular dose from phantom and patient data in mammography. Radiation Protection Dosimetry, 164 (3), pp. 342-353.

IV **Kelaranta A**, Ekholm M, Toroi P, Kortesniemi M, 2016. Radiation exposure to fetus and breasts from dental X-ray examinations: effect of lead shields. Dentomaxillofacial Radiology, 45, 20150095, pp. 1-9.

The author was primarily responsible for the literature review, data analysis and writing of the Studies I-IV. The author participated in planning of the Studies I-IV and performing the dose measurements of Studies II, III and IV and performed the Monte Carlo simulations of Study I. Study II has previously been included in the dissertation of Touko Kaasalainen (University of Helsinki, Department of Physics and Helsinki University Hospital, HUS Medical Imaging Center, Helsinki 2015). In Study II, the author prepared the phantom for the measurements and participated in performing the dose measurements led by the second author, but was in charge of the data analysis, reviewing the literature and writing the manuscript and editing it according to the co-author's comments. The results of Studies I, III and IV have not been used in other Ph.D. theses.

LIST OF ABBREVIATIONS

AAPM	American Association of Physicists in Medicine
ACR	American College of Radiology
AEC	Automatic exposure control
ALARA	As low as reasonably achievable
AP	Anterior-posterior
ATCM	Automated tube current modulation
BEIR	Biological Effects of Ionizing Radiation
BIPM	Bureau International des Poids et Mesures
BSS	Basic Safety Standards
CC	Craniocaudal
CBCT	Cone beam computed tomography
CBT	Compressed breast thickness
CDRH	Center for Devices and Radiological Health
CIRS	Computerized Imaging Reference Systems
CT	Computed tomography
CTDI	Computed tomography dose index
$CTDI_{vol}$	Volume-weighted computed tomography dose index
DAP	Dose-area product
DICOM	Digital imaging and communications in medicine
DRL	Diagnostic reference level
ESD	Entrance surface dose
FCD	Focus-to-chamber distance
FSD	Focus-to-skin distance
GSF	German National Research Center for Environment and Health
HPA	Health Protection Agency, formerly NRPB
HVL	Half value layer
IAEA	International Atomic Energy Agency
ICRP	International Commission on Radiological Protection
ICRU	International Commission on Radiation Units and Measurements

IEC	International Electrotechnical Commission
IMS	International Measurement System
ISO	International Organization for Standardization
KAP, P_{KA}	Kerma-area product
Kerma, K	Kinetic energy released per unit mass
LAT	Lateral
MGD, D_G	Mean glandular dose
MIRD	Medical internal radiation dose
MLO	Mediolateral oblique
MOSFET	Metal-oxide-semiconductor field-effect transistor
NRPB	National Radiological Protection Board, currently HPA
OSLD	Optically stimulated luminescent dosimeter
ORNL	Oak Ridge National Laboratory
PA	Posterior-anterior
PMMA	Polymethyl methacrylate
PSDL	Primary Standards Dosimetry Laboratory
ROI	Region of interest
RPLD	Radiophotoluminescent dosimeter
SD	Standard deviation
FOV	Field of view
SSDE	Size-specific dose estimate
SSDL	Secondary Standards Dosimetry Laboratory
STUK	Radiation and Nuclear Safety Authority (Säteilyturvakeskus, Finland)
TCM	Tube current modulation
TLD	Thermoluminescent dosimeter
TRS	Technical Report Series
UNSCEAR	United Nations Scientific Committee on the Effects of Atomic Radiation

AIMS OF THE STUDY

The specific aims of the research described in this thesis are

1) Compare doses to simplified patient models with doses to patients (I, III),

2) Provide measurement-based conversion coefficients for the estimation of the fetal dose in computed tomography and in dental X-ray examinations (II, IV),

3) Determine the effect of patient size (I, II, III) and radiation quality (I, III) on the dose conversion or absolute doses,

4) Determine the effect of lead shields in dental X-ray examinations during pregnancy (IV).

Study I

Kelaranta A, Toroi P, Vock P. Organ dose conversion factors in thorax X-ray examinations: the effect of patient thickness and radiation quality. Submitted in revised form to Physica Medica: European Journal of Medical Physics 3.9.2016.

Monte Carlo simulations of a thorax posterior-anterior examination were used to determine the effect of patient thickness and radiation quality on the lung and breast organ dose conversion factors. The effect of patient thickness was studied by using computed tomography (CT) examination data for adult male and female patients of different anterior-posterior thicknesses and thickness-adjusted mathematical phantoms, and the effect of different radiation qualities based on a standard-sized mathematical phantom.

Study II

Kelaranta A, Kaasalainen T, Seuri R, Toroi P, Kortesniemi M, 2015. Fetal radiation dose in computed tomography. Radiation Protection Dosimetry (2015) 165, 1-4, s. 226-230.

An adult female anthropomorphic phantom was scanned with a 64-slice CT scanner, and doses were measured with ten metal-oxide-semiconductor field-effect transistor (MOSFET) dosimeters placed inside the phantom. The fetal dose was determined in different stages of pregnancy (12, 20, 28 and 38 weeks) in trauma, abdomino-pelvic and pulmonary angiography CT protocols. Fetal dose conversion factors were calculated relative to the volume-weighted computed tomography dose index ($CTDI_{vol}$) for each pregnancy stage and CT protocol. The pulmonary angiography CT scan was used to study the effect of scan range proximity on the fetal dose.

Study III

Kelaranta A, Toroi P, Timonen M, Komssi S, Kortesniemi M, 2014. Conformance of mean glandular dose from phantom and patient data in mammography. Radiation Protection Dosimetry (2014). 164, 3, s. 342-353.

The conformance of the mean glandular dose (MGD) obtained with polymethyl methacrylate (PMMA) phantom measurements was evaluated in comparison with the MGD determined for patients in diagnostic and screening mammography based on the collected patient exposure parameters. The average compressed breast thickness from the collected patient data of Finnish women was determined and its congruence with the reference breast thickness range was evaluated corresponding to the diagnostic reference level of MGD.

Study IV

Kelaranta A, Ekholm M, Toroi P, Kortesniemi M. Radiation exposure to fetus and breasts from dental X-ray examinations: effect of lead shields. Dentomaxillofacial Radiology (2016) 45, 20150095.

Dose measurement based upper estimates of radiation exposure to the fetus and the breasts were determined in different dental X-ray examinations, including intraoral, panoramic, cephalometric and cone beam computed tomography (CBCT) examinations, both with and without lead shielding by using an adult female anthropomorphic phantom. Dose conversion coefficients were calculated as doses per the dose-area product (DAP) values of the dental examinations for a directional estimation of the dose to the fetus and breasts.

Contents

1. Introduction

Diagnostic radiology is one of the most common fields to use the benefits of X-rays. Minimizing the disadvantages of ionizing radiation is the driving force of radiation protection. A basic principle in radiation protection is the ALARA principle, which is an acronym for as low as reasonably achievable (ICRP 2007). It summarizes the approach to ionizing radiation according to the current knowledge; in the region of low doses, the probability of radiation detriment increases as a function of increasing radiation dose (ICRP 2007).

According to the most recent report, the number of X-ray examinations performed in Finland in 2011 was approximately 3.7 million, excluding dental surgery X-ray examinations (Helasvuo 2013). Of this number, approximately 9 % were computed tomography (CT) examinations and 89 % were conventional and contrast media X-ray examinations. The most common CT examinations were head, whole body, abdomen and thorax scans and the most common conventional X-ray examinations were thorax and mammography. Additionally, the number of dental radiographs taken annually in Finland is approximately 2.7 million. In 2014, the number of intraoral, panoramic, cephalometric and cone beam computed tomography (CBCT) examinations in Finland was 2.4 million, 300 000, 35 000 and 7 500, respectively (T Helasvuo, June 11, 2015, personal communication). Even though the number of X-ray examinations has decreased from 4.6 million in 1984 to 3.7 million in 2011, the number of CT examinations has increased together with the collective radiation dose accumulated from CT examinations (Helasvuo 2013; Brenner 2010).

In X-ray imaging, the patient receives a certain amount of radiation energy through absorption processes. The radiation that passes through the patient is attenuated according to the properties of the organs and tissues. The radiation sensitivities of different organs and tissues vary. The radiation energy absorbed in a tissue or an organ divided by the tissue or organ mass is the organ dose. Organ dose determination is most fundamental part of estimating the radiation risk of an individual. Organ doses cannot be measured directly and the selected method for organ dose determination has a marked impact on the uncertainty related to the organ doses.

The radiation detriment effects can be either deterministic or stochastic. Deterministic effects of radiation are related to high dose levels and cause injury and loss in populations of cells. Deterministic effects have a threshold dose below which no clinically visible effects are observed. The severity of the effect increases as a function of dose. Stochastic effects consist of cancer risk and hereditary effects, and the probability of an effect, but not its severity, increases as a function of dose without a threshold (ICRP 2007). The radiation effect classification, dose limitation concepts, and the definition of detriment and threshold have undergone several changes in the past decades (Hamada & Fujimichi 2014).

The International Commission on Radiological Protection (ICRP) has defined and introduced the concept of effective dose for risk management purposes, and the tissue weighting factors for the calculation of the effective dose. The tissue weighting factors are based on epidemiological cancer incidence studies and risk estimation of hereditary diseases (ICRP 2007). Initially, the tissue weighting factors are based on atomic bomb survivor data

with whole-body exposures, but in X-ray imaging organs and tissues receive partial or heterogeneous exposure. The tissue weighting factors are intended to apply to a population of both genders and all ages, not for an individual. The tissue weighting factors change every decade or so due to increased knowledge about radiation effects, but also because different ICRP committees might chose to put more emphasis on for example cancer incidence rather than cancer mortality. The latter is the case for breast, the tissue weighting factor of which has increased from 0.05 to 0.12 in ICRP publications 60 and 103, respectively (ICRP 1991; ICRP 2007).

However, there has been criticism and discussion of the concept of effective dose (Brenner 2008; Dietze et al. 2009; Brenner 2012). It has often been misused and the confusion between equivalent dose and effective dose is widespread in the field of radiology. Proposal of a replacing quantity has been made (Brenner 2008; Brenner 2012), but the concept of the effective dose still remains in radiation protection. It has been stated that the individual organ dose is a better measure for estimating the patient risk, because the effective dose is intended for estimating the radiation exposure of entire populations and not for individuals (Brenner & Hall 2007; Martin 2007; Zhang et al. 2012; Hall & Brenner 2008; Brenner et al. 2003). In some of the recent publications, the organ doses are used in the estimation of the patient risk instead of the effective dose (Blaszak & Juszkat 2014; Saltybaeva et al. 2016), but as the effective dose is a traditional dose quantity, it is still being commonly used in the literature. Moreover, the United Nations Scientific Committee on the Effects of Atomic Radiation (UNSCEAR) has strongly emphasized, that the effective dose is not directly applicable to interpretation of data on health effects because it is developed for radiation protection purposes (UNSCEAR 2008a; UNSCEAR 2008b). However, it can be used to allow comparison of different types of examinations, equipment and technique factors from a risk point of view, but there is no need to quantify any risk coefficients as the detriment or risk per effective dose (IAEA 2007).

This thesis concentrates on organ dose determination based on dose measurements or Monte Carlo simulations in four diagnostic X-ray imaging modalities: general radiography, CT, mammography and dental radiography. The differences between doses to patients and simplified patient models are compared in mammography and general radiography. The effect of patient size on the dose conversion coefficients or absolute doses is determined in general radiography, CT and mammography and the effect of radiation quality on the dose conversion coefficients or absolute doses is determined in general radiography and mammography. Results on measurement based conversion coefficients are given for fetal dose estimation in CT and dental X-ray examinations and the effect of lead shielding in dental X-ray examinations is determined.

2. Background

2.1. Dose quantities

The dose quantities can be divided into basic dosimetric quantities, application specific dosimetric quantities and quantities related to stochastic and deterministic radiation effects (IAEA 2007; ICRU 2005). The relevant basic dosimetric quantities in this thesis are the kerma K and the absorbed dose D. The relevant application specific dosimetric quantities are the incident air kerma $K_{a,i}$, the entrance air kerma $K_{a,e}$, the X-ray tube output Y(d), the air kerma–area product, KAP or P_{KA}, the air-kerma-length product P_{KL} and CT air kerma

indices. The relevant quantities related to stochastic and deterministic radiation effects are the organ dose D_T, the equivalent dose H_T, the effective dose E and the mean glandular dose (MGD or D_G). This thesis introduces the dosimetric quantities and uncertainty estimation according to Technical Report Series (TRS) publication No. 457 and report No. 74 of the International Commission on Radiation Units and Measurements (ICRU) (IAEA 2007; ICRU 2005). In this thesis, the term *uncertainty* is preferred over the term *accuracy*, because the term *accuracy* assumes that the true value of some quantity can be exactly measured, which is not possible in reality. The relevant dose quantities are shown in Figure 1.

The kerma (kinetic energy released per unit mass) K is the sum of the initial kinetic energies of all the charged particles liberated by uncharged particles, dE_{tr}, in a mass dm of material, and it is defined as

$$K = \frac{dE_{tr}}{dm} \tag{1}$$

The absorbed dose D is the mean energy $d\bar{\varepsilon}$ imparted to matter of mass dm, and it is defined as

$$D = \frac{d\bar{\varepsilon}}{dm} \tag{2}$$

In the case of charged particle equilibrium, the numerical values for K and D are equal.

The air kerma K_a is measured free in air at the focus-to-chamber distance (FCD), and can be corrected to represent the incident air kerma $K_{a,i}$ measured on the central beam axis at the position of the patient or phantom surface at focus-to-skin distance (FSD) by using the inverse-square law. Only the radiation incident on the patient or phantom is included in $K_{a,i}$.

$$K_{a,i} = K_a \left(\frac{FCD}{FSD}\right)^2 \tag{3}$$

The assumptions for Equation (3) include air attenuation of photons at the zero level, which is strongly dependent on the energy. Also, scattered radiation in the primary beam is excluded.

The entrance surface air kerma, $K_{a,e}$, is the kerma to air measured on the central beam axis at the position of the patient or phantom surface. The radiation incident on the patient or phantom and also the backscattered radiation are included. The entrance surface air kerma $K_{a,e}$ is related to the incident air kerma $K_{a,i}$ by the backscatter factor B

$$K_{a,e} = K_{a,i} B \tag{4}$$

The X-ray tube output, Y(d), is defined as the quotient of the air kerma at a specified distance, d, from the X-ray tube focus by the tube current–exposure time product, P_{It}, as

$$Y(d) = \frac{K(d)}{P_{It}} \tag{5}$$

The air kerma–area product, KAP or P_{KA}, is the integral of the air kerma over the area A of the X-ray beam in a plane perpendicular to the beam axis. In this thesis, the more commonly used abbreviation, the dose-area product (DAP) is used. The air-kerma length product, P_{KL}, is the integral of the air kerma over a line L parallel to the axis of rotation in a CT scanner

$$P_{KA} = \int_A K_a(A)dA \tag{6}$$

$$P_{KL} = \int_L K_L(L)dL \tag{7}$$

The most important quantities for CT dosimetry are the CT air kerma index, $C_{a,100}$, the weighted CT air kerma index, C_W and the volume-weighted CT air kerma index, C_{VOL}, which takes into account the helical pitch or axial scan spacing p. In this thesis, the more commonly used abbreviation for C_{VOL}, the volume-weighted CT dose index ($CTDI_{vol}$) is used when referring to the original publications.

$$C_{a,100} = \frac{1}{T}\int_{-50}^{50} K(z)dz \tag{8}$$

$$C_W = \frac{1}{3}\left(C_{PMMA,100,c} + 2C_{PMMA,100,p}\right) \tag{9}$$

$$C_{VOL} = \frac{C_W}{p} \tag{10}$$

The organ dose D_T is a quantity recommended by the ICRP as the appropriate dosimetric indicator for the probability of stochastic radiation effects (ICRP 1992). D_T is defined as the absorbed dose averaged over an organ, i.e., the ratio of the total energy imparted to the tissue or organ, $\bar{\varepsilon}_T$, to the total mass of the tissue or organ, m_T.

$$D_T = \frac{\bar{\varepsilon}_T}{m_T} \tag{11}$$

The effective dose E is defined as the weighted sum of the organ doses. The weighting factors are the tissue weighting factor w_T and the radiation weighting factor w_R.

$$E = \sum_T H_T = \sum_T w_T \sum_R w_R \cdot D_{T,R} \tag{12}$$

The mean glandular dose MGD or D_G is recommended (ICRP 1987; ICRU 2005) for breast dosimetry in diagnostic radiology. It is defined as

$$D_G = K_{a,i} \cdot g \cdot c \cdot s, \tag{13}$$

where g is the conversion factor that considers the radiation quality and breast thickness (50 % glandularity). Correction factors s and c are for the spectra and glandularity, respectively. When no glandularity correction is applied, c = 1.

Conversion coefficients can be used for the assessment of organ and tissue doses. They relate the dose to an organ or tissue to a directly measured or calculated dosimetric quantity, such as $K_{a,i}$, $K_{a,e}$, P_{KA} or C_{VOL}. Conversion coefficient is defined as

$$\text{conv. coeff.} = \frac{D_T}{\text{measured or calculated quantity}} \quad (14)$$

According to the standard ISO 31-0 (ISO 1992) and its revision, ISO 80000-1 (ISO 2009), the term *coefficient* should be used for a multiplier possessing dimensions, and the term *factor* for a dimensionless multiplier. This convention is not always obeyed consistently in the literature. In this thesis the term *conversion coefficient* is used throughout when *conversion factors* and *conversion coefficients* are referred to.

Diagnostic reference levels (DRLs) are provided by the national radiation authorities according to the requirements of the Basic Safety Standards (BSS), and they are introduced in legislation (European Parliament 2014). The BSS require the use of DRLs as a part of the optimization of the protection of patients in diagnostic radiology (IAEA 2014). The DRL defines the radiation dose level that is not expected to be exceeded for a normal-sized patient in an examination performed according to good practices. DRLs are used in the management of patient doses in order to ensure that in diagnostic radiology, the dose levels of a selected patient cohort, which is selected based on weight or compressed breast thickness (CBT) information, are adequate yet not too high for the required diagnostic information. The dosimetric quantities recommended for the establishment of DRLs are $K_{a,i}$, $K_{a,e}$, D_G, P_{KA} and P_{KL} (ICRU 2005).

The uncertainty of measurement results is typically expressed as expanded uncertainty using coverage factors. The combined standard uncertainty u_C is defined as

$$u_C = \sqrt{{u_A}^2 + {u_B}^2}, \quad (15)$$

where u_A and u_B are the standard uncertainties of type A and B, respectively. Equation (15) is valid when the uncertainty sources are not correlated. In the general variance model, this results in zero covariance. Generally, for a product or ratio of independent variables, the relative weighted variances add, and this is expressed in the propagation of uncertainties as a square root of an infinite sum of the squared weights and the squared relative uncertainties. (IAEA 2007)

Type A standard uncertainty is the standard deviation (SD) of the mean from a series of repeated measurements. Type B standard uncertainty takes into account all sources of measurement uncertainty that cannot be estimated by repeated measurements. These can be physical uncertainties, such as uncertainty related to positioning of the phantoms and dosimeters, X-ray beam intensity, X-ray spectra (in relation to the dosimeters's response) and the angular dependency of dosimeters. The expanded uncertainty U is obtained by multiplying u_C by a coverage factor k.

$$U = k \cdot u_C \quad (16)$$

Typically, k is in the range 2 to 3. When the normal distribution applies, coverage factor k = 2 defines an interval having a confidence level of approximately 95% and k = 3 defines an interval having a confidence level of greater than 99 %. (IAEA 2007)

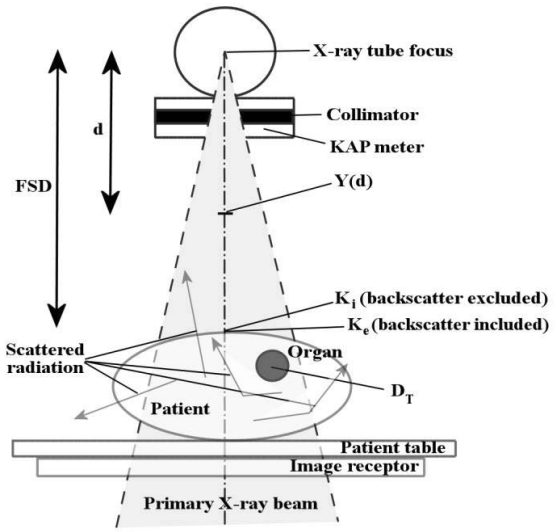

Figure 1 *The relevant dose quantities in patient dosimetry in projection X-ray imaging, according to TRS 457 (IAEA 2007). The abbreviations are defined in the text.*

2.2. Imaging modalities

This thesis concentrates on four important diagnostic imaging modalities: general radiography, CT, mammography and dental radiography. The level of organ exposure to X-ray radiation depends on the part of the body being in the primary radiation beam, imaging parameters, patient anatomy, radiation quality and the use of radiation shields. The specific uncertainties related to each modality examined in this thesis are reviewed briefly according to TRS No. 457 (IAEA 2007) and ICRU report No. 74 (ICRU 2005).

In general, the largest sources of measurement uncertainty in diagnostic dosimetry are the quantities related to the direct measurements, namely the intrinsic error, the difference in the radiation quality between Secondary Standards Dosimetry Laboratory (SSDL) or calibration laboratory and the user, the direction of the radiation incidence, the kerma rate, the operating tube voltage, the environmental parameters (air pressure, temperature, humidity and electromagnetic compability), the field size and homogeneity and the long term stability of the instruments. (IAEA 2007)

2.2.1. General radiography

General radiography is one of the most basic forms of medical X-ray imaging and it utilizes single projections to produce two-dimensional images based on the different attenuation properties of tissues and organs. Contrast medium is not used general radiography. The term *conventional radiography* is also used for non-contrast media X-ray examinations, but it includes mammography. In single projection imaging, the dose to an organ is high on the X-ray beam's entrance side and low at the exit side.

Radiological examination of the thorax is one of the most common diagnostic X-ray examination (Helasvuo 2013; Speets et al. 2006; Veldkamp et al. 2009). The thorax can be examined in different projections: posterior-anterior (PA), anterior-posterior (AP) and lateral (LAT). Thorax PA projection has the advantage of lower absorbed dose to the radiosensitive breast tissue compared to the AP projection, where the breasts are at the patient entrance where the absorbed dose is highest (Huda & Gkanatsios 1997). Filtration of the X-ray beam is used to eliminate the low energy photons that would otherwise increase the radiation dose absorbed by the patient. The effect of filtration is seen at the patient entrance, and would decrease the dose to the breasts in AP projection. However, the PA projection is the standard chest radiograph in standing position together with LAT projection; AP projection may be used instead of PA projection in standard examinations if the patient is too unwell to stand (Radiology Masterclass 2016).

In this thesis, general radiography is examined via Monte Carlo simulations without dosimetric measurements. The uncertainties in Monte Carlo simulations originate primarily from statistical errors. Statistical uncertainties in the doses to organs that are within the X-ray beam are less than those for organs outside the beam area. In the latter case, the relative uncertainty increases with the distance from the scan range. The number of primary photons used in the simulation defines the level statistical uncertainties. Other sources of uncertainties in Monte Carlo simulations are uncertainties in the attenuation coefficients and inadequacies in the model description of the X-ray source and the patient. (ICRU 2005)

2.2.2. Computed tomography

Computed tomography utilizes combinations of multiple X-ray projections to produce cross-sectional tomographic images of specific areas of the patient. The dose quantities used in CT, namely $C_{a,100}$, C_W, C_{VOL} and P_{KL} are defined in standard-sized cylindrical polymethyl methacrylate (PMMA) phantoms. The standard cylindrical head and body phantoms have diameters of 16 cm and 32 cm, respectively. The internal phantom and patient dose distributions are more uniform in CT than in projection imaging. However, the CT dose quantities do not correspond to the patient doses, because they cannot consider the different patient sizes, genders and patient anatomy. The CT dose quantities are useful in estimating the effects of parameter changes to the dose and in comparing protocols between different CT devices.

This thesis concentrates on CT examinations during pregnancy. The most common indication for chest CT during pregnancy is suspected pulmonary embolism, whereas for abdomino-pelvic CT, the two most common indications are suspected appendicitis and trauma (Goldberg-Stein et al. 2011). These indications include both situations where the fetus is completely or partly within the scan volume, or outside of it.

The specific sources of measurement uncertainties in computed tomography are the precision of reading and tube loading indication, the precision of chamber and phantom positioning in the centre of gantry, the uncertainties related to the phantom diameter and the depths of measurement bores and the uncertainty in chamber response for measurements inside the phantom (IAEA 2007).

2.2.3. Mammography

Mammography is a specific type of breast X-ray imaging that uses low energy X-rays to detect cancer typically before women experience symptoms. Early detection allows treatment at the point when the breast cancer is the most treatable. Standard projections (views) in mammography are craniocaudal (CC) projection and mediolateral oblique (MLO) projection, which are usually performed on routine screening mammograms for all patients. The projection angles in the CC and MLO views are 0º and 45º, respectively. Breast compression is used in mammography, because it reduces both breast thickness and radiation dose and increases image quality. MGD is the relevant dose quantity in mammography, and it is the dose to the glandular tissue of the breast, being dependent on the measurable incident air kerma at the patient breast surface, the breast thickness and glandularity and the applied radiation quality. Furthermore, CBT is the relevant patient thickness in mammography.

In mammography, a PMMA phantom of 45 mm thickness is generally used and recommended to simulate the standard breast of thickness 50 mm and glandularity of 50 % (ICRU 2005; European Commission 2006; IAEA 2007; Fitzgerald 1989). PMMA equivalent breast thicknesses have been calculated by Dance et al. (Dance 1990; Dance et al. 2000) for CBTs of 20 to 110 mm. Furthermore, Dance et al. (Dance 1990; Dance et al. 2000; Dance et al. 2011) have determined the most recent conversion and correction factors for mammography with Monte Carlo simulations, and they are internationally (European Commission 2006; IAEA 2007) and nationally (Toroi et al. 2011) recommended for the calculation of MGD. This thesis focuses on the differences in the determined MGD for patient and phantoms of different thicknesses.

The specific sources of measurement uncertainties in mammography are the precision of reading and tube loading indication, the uncertainty in measurement position, the uncertainties related to half value layer (HVL) measurements and the uncertainty in patient or phantom thickness (IAEA 2007).

2.2.4. Dental radiography

Dental radiography includes different sub-modalities that are used for different purposes. Intraoral radiography is used to produce an X-ray image of a single tooth or a couple of teeth. Panoramic dental examinations provide an image of the whole maxilla and mandible, and cephalometric dental examinations are used in orthodontics. CBCT dental examinations are a special type of x-ray equipment used when regular dental or facial x-rays are not sufficient. CBCT produces three dimensional (3D) images of the teeth and bones in a single scan. The highest doses in dental radiography are in the head and neck region; doses in other regions are mainly due to scattered radiation. The focus of this thesis is in the radiation doses to the fetus and breasts in dental radiography with and without lead shielding.

The specific sources of measurement uncertainties in dental radiography are the precision of reading and the uncertainty in measurement position (IAEA 2007).

2.3. Organ dose determination

Accurate estimation of organ doses requires detailed modelling of the patient anatomy and the irradiation field (Samei et al. 2014). Patient anatomy depends on the patient size and composition, which affect the organ sizes and positions inside the body. The patient size can be characterized for example by the mass, height, body mass index or thickness of the patient. Also thickness of a certain part of the patient, such as the breast, or size related parameters calculated based on the AP and LAT thicknesses can be used to represent the patient size. The characterization of the irradiation field in projection imaging considers the projection, the field size and the radiation quality, and in CT the tube current modulation (TCM) technique, radiation quality, the bowtie filter and the scan range need to be considered. The radiation quality can be characterized by the X-ray spectrum. The X-ray spectrum is a representation of the radiation intensity as a function of the photon energy and the characteristic peaks in the spectrum are defined by the anode material and the maximum energy is determined by the tube voltage. Filtration of the spectrum modifies the shape of the spectrum, for example by eliminating low energy photons. The parameters and properties used to characterize a radiation quality are the anode properties, the HVL, the X-ray tube voltage and the total filtration (ICRU 2005).

The first difficulty in organ dose determination is that it cannot be measured directly in patients, because it would require installation of internal dosimeters in patient's organs and would not be ethically acceptable. There are various methods available for patient organ dose estimation and determination. The coarsest and least accurate level of dose estimation is to use average or typical tabulated dose value of the examination. The second level are organ dose conversion coefficients, that are typically determined based on measurements in physical phantoms or Monte Carlo simulations, and the use of conversion coefficients allow considering the measurable incident dose. Monte Carlo simulations are the better established approach for organ dose conversion coefficient determination, because they are well validated and they have the important advantage of flexibility compared to phantom measurements (IAEA 2007). The conversion coefficients are the most accurate when they are selected based on the information of the patient anatomy and the exposure situation, and when the real and the simulated situations match as closely as possible. However, the conversion coefficients available do not necessarily cover the case where organ dose estimation is needed. Anthropomorphic phantom measurements and Monte Carlo simulations that apply straight for the specific case provide a more accurate method for organ dose determination, and are especially useful for certain special situations, such as pregnant patients.

The most accurate and time consuming method is to use patient specific organ dose determination based on dose simulations on the actual CT data of the patient. This approach is commonly used in radiation therapy dose calculations, but not in patient dosimetry in diagnostic radiology on a routine basis. The organ dose assessment in diagnostic radiology is usually made for particular practices and techniques, that are applied to a large number or patients, and therefore there is not the same need for individually tailored patient dose determination as in radiation therapy (ICRU 2005). This has led to the use of standard patient models in diagnostic radiology, but recently patient size-specific dose estimates (SSDEs) have been developed for CT by the American Association of Physicists in Medicine (AAPM 2011). For projection radiography, similar patient size-specific dose estimates are not yet in general use.

2.3.1. Dose detectors and dosimeters

In medical dosimetry, dose detectors and dosimeters are used for example to detect and measure the radiation dose inside or outside a subject that is exposed to ionising radiation, or the tube output or air kerma of an X-ray device. The selection of an appropriate dose measurement device depends on the situation; are the measurements done in the primary radiation beam, or does the device see only scattered radiation.

Ionization chambers are gas-filled chambers with two electrodes: anode and cathode. They measure the charge from the number of electron-ion pairs created by incident radiation within the gas volume (Knoll 2000). There are many different sized and shaped ionization chambers for different purposes. In CT, pencil ionization chambers are used in CTDI and air kerma measurements. Air kerma measurements in mammography can also be performed by low energy ionization chambers.

Solid state detectors are based on semiconductors, and they resemble ionization chambers by their operation, but instead of electron-ion pairs, radiation generates electron-hole pairs in the semiconducting material, which is usually silicon or germanium. A number of electrons are transferred from the valence band to the conduction band, and the same number of holes is created in the valence band. However, this is the situation in a completely pure semiconductor; in real materials the electrical properties are dominated by very small levels of residual impurities (Knoll 2000). Solid state dosimeters can be used for example in tube output and scattered radiation dose measurements

Other types of dosimeters used in medical dosimetry are thermoluminescent dosimeters (TLDs), radiophotoluminescent dosimeters (RPLDs), optically stimulated dosimeters (OSLDs) and metal-oxide-semiconductor field-effect transistors (MOSFETs) (Ristic 2013; Manninen 2014; Yoshizumi et al. 2007; Kaasalainen 2015). All these dosimeter types can be used to perform organ dose measurements inside anthropomorphic phantoms. MOSFET dosimeters allow immediate readout after radiation exposure, which is not feasible with TLDs (Yoshizumi et al. 2007). MOSFET dosimeters consist of an insulating layer of silicon dioxide (SiO_2), a silicon semiconductor substrate and a polycrystalline silicon or metal gate, and their operation is based on electron-hole pairs created by ionizing radiation and the resulting change in the threshold voltage required to turn on the transistor (Knoll 2000; Brady & Kaufman 2012). When MOSFET dosimeters are used with multiple angles of irradiation, their angular dependence must be considered. Variation in the angular sensitivity of MOSFET dosimeters has been observed, and therefore they should always be calibrated in the actual clinical settings for the beam geometry (Koivisto et al. 2013).

Traceability is by definition a continuous calibration chain, in which all stages have estimated uncertainties. The traceability of the measured doses to the primary standards is provided by the International Measurement System (IMS) for radiation metrology. The IMS consists of the Bureau International des Poids et Mesures (BIPM), national Primary Standards Dosimetry Laboratories (PSDLs), Secondary Standards Dosimetry Laboratories (SSDLs) and radiation users performing measurements (IAEA 2007). International Atomic Energy Agency (IAEA) has also a SSDL laboratory and maintains a worldwide network of SSDLs. The calibration of radiation instruments used in medical dosimetry is usually performed in SSDLs, but calibration services are also provided by the instrument manufacturers. In Finland, the Radiation and Nuclear Safety Authority (STUK) is a part of

the SSDL. Calibrations of detectors in medical use should be performed at the SSDL on a routine basis. Standard radiation qualities are recommended for the calibration of dosimeters used in different imaging modalities (IEC 2005; ICRU 2005; IAEA 2007). However, in clinical situations the radiation quality can be different from radiation quality used in the calibration.

2.3.2. Anthropomorphic phantoms

One challenge in patient organ dose determination is to mimic the human anatomy accurately enough to provide a model for dosimetry. Anthropomorphic phantoms used in medical dosimetry can be divided into computational phantoms and physical phantoms. Computational phantoms are either mathematical or voxel phantoms. By the end of 2009, approximately 121 computational phantoms and 27 physical phantoms have been reported in the literature for studies involving ionizing and non-ionizing radiation (Xu & Eckerman 2009). The majority of the computational phantoms, 84, were constructed from CT or MRI images of live subjects or cross sectional photographs of post-mortem subjects (Xu & Eckerman 2009).

The first human-like, i.e. anthropomorphic mathematical phantom was developed by Fisher and Snyder at Oak Ridge National Laboratory (ORNL) in 1960s (Fisher & Snyder 1966; Fisher & Snyder 1967). The work in ORNL continued, and in 1969, the first heterogeneous phantom was reported, and it became known as the "MIRD-5 Phantom" (Snyder, Fisher, et al. 1969; Snyder, Ford, et al. 1969). The organ masses were selected to follow as closely as possible the data of the ICRP Reference Man (ICRP 1975). The MIRD (Medical Internal Radiation Dose) phantom has been the basis for numerous derivations representing for example family phantom series (Cristy & Eckerman 1987), infants and children of different ages (Cristy 1980), gender-specific adult phantoms ADAM and EVA (Kramer et al. 1982) and later in 1990s also pregnant female adult phantom (Stabin et al. 1995). The body and the organs in the MIRD phantom are simple, geometrical shapes, which is an inborn limitation of mathematical phantoms. Many anatomical details in mathematical phantoms are compromises that can in some cases lead to inaccurate results (Xu 2014). However, the role of mathematical phantoms remain important, and they are used in recent publications (Seidenbusch & Schneider 2014; Damilakis, Tzedakis, et al. 2010).

More realistic voxel phantoms were introduced in the late 1980s, when powerful computer and tomographic imaging technologies became available. Voxel phantoms are called the second generation phantoms to separate them from the first generation mathematical phantoms. Voxel phantoms are based on CT or magnetic resonance imaging (MRI) data from which the organs are segmented. In 1990s, two adult male voxel models were developed: Voxelman (Zubal 1999) and NORMAN (Dimbylow 1997). The VIP-Man (Xu et al. 2000) was the most complex phantom to date, with over 3.7 billion voxels. The GSF family of voxel phantoms consists of both pediatric (Veit et al. 1989) and adult phantoms of both sexes, different ages and body size (Petoussi-Henss et al. 2002), and it is the most comprehensive series of voxel phantoms. Also adult female voxel phantoms representing different nationalities have been developed (Dimbylow 2005; Sheng et al. 2013; Sato et al. 2009). After the construction of the adult and pediatric phantoms, phantoms representing different pregnancy stages (Xu et al. 2007; Dimbylow 2006) and phantoms of newborn babies (Lee et al. 2007) have been developed. Furthermore, ICRP Reference Male and Female voxel phantoms have been constructed in 2009 that resemble the ICRP 89 reference values for their body height, weight and organ masses (Zankl & Wittmann 2001; ICRP

2002; ICRP 2009). The ICRP Reference Male and Female phantoms are defined to enable calculations of the organ and tissue equivalent doses and the effective dose. Voxel phantoms that include the whole human body have been used also in mammography (Tzamicha et al. 2015) and dental radiography (Morant et al. 2013). Dynamic phantoms have also been developed that simulate the cardiac and respiratory motion or variable postures (Segars et al. 2010; Nagaoka & Watanabe 2009). Many of the most recent phantoms are based on the powerful boundary representation methods, which is different from the constructive solid geometry method used in earlier voxel phantoms (Xu 2014).

While mathematical and voxel phantoms are typically used in simulation programs, physical anthropomorphic phantoms can also be used in Monte Carlo simulations and dose measurements. Physical phantoms contain small cavities for dose measurement devices, such as MOSFET dosimeters or TLD dosimeters. For example, CIRS ATOM phantoms of different sizes (Computerized Imaging Reference Systems, Norfolk, VA, USA) include adult male and female phantoms and pediatric newborn, one-year-old, five-year-old and ten-year-old phantoms. There is also CIRS ATOM Max dental and diagnostic head phantom to be used as a standard of reference for diagnostic radiology of the head. Other commercially available physical anthropomorphic phantoms are for example the RANDO phantom (The Phantom Laboratory, Salem, NY, USA) and Alderson ART phantoms (Radiology Support Devices, Long Beach, CA, USA). In mammography, non-anthropomorphic PMMA breast phantom proposed by Dance is recommended for evaluating the glandular dose in a standard breast, but several other models have also been developed (Cassola & Hoff 2010).

2.3.3. Monte Carlo simulations

Monte Carlo simulations are widely used in medical dosimetry. The general requirements of a Monte Carlo model are the simulation of the radiation field incident on the patient, the photon transport through the patient and the patient anatomy (IAEA 2007; ICRU 2005). In medical X-ray imaging, the simulated photon interactions are the photoelectric effect and coherent and incoherent scattering because the incident photon energies are below 150 keV (ICRU 2005). Voxel-based Monte Carlo simulations require characterization and modelling of the X-ray device and patient anatomy (Gu et al. 2009; Ding et al. 2012; Lee et al. 2011; Bostani et al. 2015; Tian et al. 2014; Sinclair et al. 2015; Li et al. 2011a). Modelling of the X-ray device requires data for the X-ray spectrum and in CT also for the bowtie filter. Furthermore, Monte Carlo simulations may require for example measurement results for air kerma quantities (such as K_a or P_{KA}) as the input value. The simulation results can therefore be presented as conversion coefficients relative to the input value. All conversion coefficients depend on the radiation quality and they are most accurate when the simulated situation matches as closely as possible the situation in which the organ doses are required (IAEA 2007).

Three institutes that have published the most comprehensive tabulations of organ dose conversion coefficients are the Center for Devices and Radiological Health (CDRH), the German Center for Health and the Environment (GSF) and the Health Protection Agency (HPA), formerly the National Radiological Protection Board (NRPB) (ICRU 2005). These comprehensive tabulations of organ dose conversion coefficients have been determined by Monte Carlo simulations, because they are more applicable than measurements in physical phantoms when a wide variety of clinical situations or exposure conditions need to be

considered (ICRU 2005). However, comparisons between these simulations and measured organ doses have been made, and agreement was generally within 30 % for adult phantoms and within 40% for paediatric phantoms (ICRU 2005). Additionally, several authors have published Monte Carlo simulation based organ dose conversion coefficients for various exposure situations (e.g. Zankl et al. 2002; Schlattl et al. 2007; Turner et al. 2011; Seidenbusch & Schneider 2014; Johnson et al. 2009; Schultz et al. 1994; Lee et al. 2012; Petoussi-Henss et al. 2002). In some cases, doses have been normalized only to the P_{lt}, which make it hard to compare the dose conversion coefficient with those normalized to for example C_{VOL}.

The data provided by the GSF and the NRPB have been used in patient dose calculation programs. For example, the ImPACT CT Patient Dosimetry Calculator (IMPACT 2011) uses the NRPB data and CT-Expo (Stamm & Nagel 2002) uses the GSF data. Patient models used in Monte Carlo calculation and simulation programs can be either mathematical or voxel phantoms. Some of the calculation programs include assumptions about the beam positioning and they use a standard-sized phantom. For example, XDOSE (Le Heron 1994) is based on the organ doses generated by the Monte Carlo method described in NRPB-R262 and NRPB-SR262 (Hart et al. 1994a; Hart et al. 1994b). CALDose_X (Kramer et al. 2008) provides an improved patient model by using male and female voxel phantoms instead of a standard MIRD-type geometrical patient model used in NRPB-R262 and NRPB-SR262 (Hart et al. 1994a; Hart et al. 1994b). PCXMC program (Tapiovaara & Siiskonen 2008) includes hermaphrodite mathematical phantoms of ages 0, 1, 5, 10, 15 and adult. Principal weights and heights of these phantoms are based on the specifications by Cristy & Eckerman (1987), which have been modified for PCXMC. ImpactMC program from CT Imaging, Erlangen, Germany (Deak et al. 2008; Schmidt & Kalender 2002) allows the user to generate 3D dose distributions in CT data of phantoms or patients with user-defined acquisition parameters. Several public domain Monte Carlo code systems that can be applied to medical dosimetry include for example MCNP (X-5 Monte Carlo Team 2003), MCNPX (Pelowitz 2008), EGSnrc (NRC 2016), Geant4 (Agostinelli et al. 2003; Allison et al. 2006), PENELOPE (Baró et al. 1995) and Fluka (Battistoni et al. 2007). The large variety of mathematical, voxel and physical phantoms available can be used in different Monte Carlo simulation programs, which expands the possibilities of organ dose determination in medical dosimetry.

3. Materials and methods

In this thesis, four different imaging modalities were used, and each one is covered by one study. Some of the modalities include also sub-modalities. The X-ray devices, imaging protocols, phantoms, patient data, performed dose measurements, Monte Carlo simulations and calculations related to Studies I-IV are presented.

3.1. General radiography

In Study I, mathematical phantoms and patient CT data were used in Monte Carlo simulations with imaging parameters for thorax PA examination. Monte Carlo programs

used were PCXMC 2.0 (Tapiovaara & Siiskonen 2008) and ImpactMC (version 1.4.0.0, 2014) from CT Imaging, Erlangen, Germany (Deak et al. 2008; Schmidt & Kalender 2002). The X-ray spectra used in PCXMC simulations was generated in PCXMC. The X-ray spectrum used in ImpactMC simulations was generated using Spektripaja 3.0 (Tapiovaara & Tapiovaara 2008), which is based on a semiempirical spectrum model (Birch & Marshall 1979). In PCXMC simulations, incident air kerma of 1 mGy was used as an input value and in ImpactMC simulations, fixed air kerma of 1 mGy was used as an input value and the incident air kerma at the FSD was calculated based on the patient thickness.

In Study I, anonymized patient CT data for 5 male and 5 female adult patients investigated in 2011 at the Inselspital University Hospital, Bern, Switzerland were used. CT data sets for these 10 patients and mathematical PCXMC phantoms thickness-adjusted according to the male patients were used in ImpactMC and PCXMC programs, respectively, in order to study the effect of patient thickness. In Figures 2 and 3, examples of ImpactMC and PCXMC simulations are shown, respectively. The patient selection criteria were that the patients had undergone trauma CT, the scanned region covered the lungs and both genders were represented equally by 5 five different body sizes, ranging from extra small to small, medium, large, and extra large. The patient thickness measured at the mid-sagittal plane at the mamilla level in the anterior–posterior (AP) dimension was used to define the patient size. The effect of radiation quality was determined in PCXMC for a standard-sized PCXMC phantom with four different filtration combinations and a range of tube voltages and the corresponding HVLs.

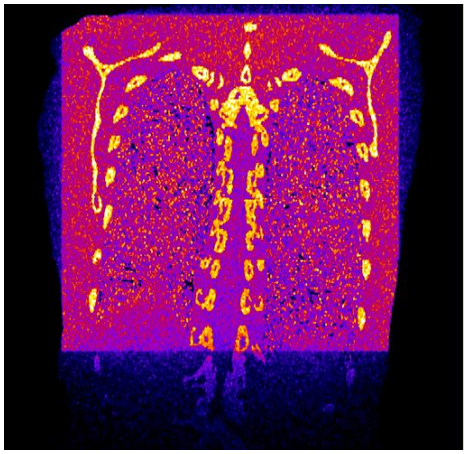

Figure 2 *ImpactMC simulation of thorax posterior-anterior (PA) examination in Study I.*

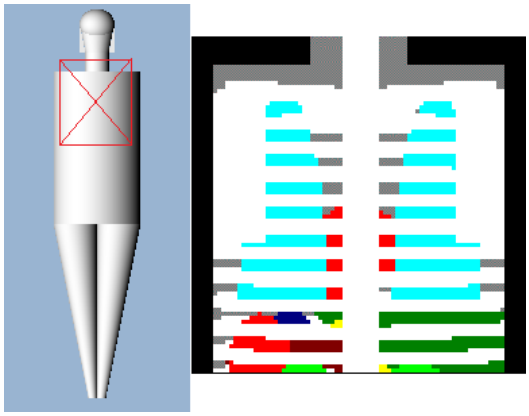

Figure 3 *Thorax posterior-anterior (PA) examination on the PCXMC phantom in Study I.*

In Study I, doses from ImpactMC simulations were determined at the mamilla level from circular regions of interest (ROIs) in ImageJ (Abramoff et al. 2004) at two different depths (back and sternum positions) in the X-ray beam's trajectory. The position and size of the ROIs were adjusted patient-specifically so that the dose distribution inside the ROI area was uniform. Computer programs 3DSlicer (version 4.4) and Matlab (version R2014b) were used in the segmentation of lungs and breasts from the patient CT data. Breasts were segmented for the female patients only and organ doses were determined from the resulting volumes of interest (VOIs). In PCXMC, the absorbed doses to lungs and breasts were determined as organ doses. Dose conversion coefficients were calculated by dividing the ROI doses from ImpactMC simulations and organ doses from ImpactMC and PCXMC simulations by the incident air kerma and expressed in µGy/100 µGy. The reference conversion factors were calculated for the PCXMC phantom with standard dimensions. The relative variation ranges of the conversion coefficients were calculated as the difference between the maximum and minimum values relative to the mean value and the reference value.

3.2. Computed tomography

In Study II, CT imaging protocols for trauma, low dose abdomino-pelvic and pulmonary angiography were used. 64-MDCT GE LightSpeed VCT scanner (GE Healthcare, Milwaukee, WI, USA) was used and the normal clinical examination was simulated as closely as possible. Three different pregnancy stages (20, 28, 38 weeks) were constructed by positioning gelatin boluses on the anthropomorphic adult female phantom (CIRS ATOM 702-D, Norfolk, USA), as shown in Figure 4 for the pregnancy stage of 38 weeks. A phantom with no bolus represented the pregnancy stage of 12 weeks and non-pregnancy stage.

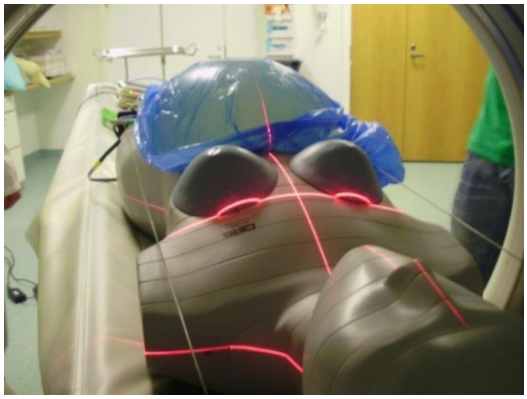

Figure 4 *CIRS ATOM 702-D phantom and the 38-week gelatin bolus in Study II.*

Prior to the measurements of Study II, ten high sensitivity MOSFET dosimeters were calibrated for the energies used in the dose measurements in a clinical CT beam using axial scan mode and dose values were registered using a mobileMOSFET 2.4.1. Dose Verification System (TN-RD-70-W, Best Medical, Canada). In the calibrations, the reference CT air kerma indices ($C_{a,c}$) were measured with a RaySafe Xi base unit and a RaySafe Xi CT detector (Unfors RaySafe AB, Billdal, Sweden) and calibration factors were defined for each of the ten MOSFET dosimeters. In general, the MOSFET calibration procedure can be performed by using different methodologies (Brady & Kaufman 2012).

In Study II, the MOSFET dosimeters were placed inside the phantom at nine measurement positions (Figure 5, positions B-J), and one dosimeter was placed beneath the centre of the bolus on the phantom surface (Figure 5, position A). Measurement positions were selected to cover relevant uterus dimensions for all stages of pregnancy considering the possible fetal positions. The mean fetal dose was determined for each stage of pregnancy by averaging the measured doses corresponding to the estimated uterus volume. Conversion coefficients were calculated for each stage of pregnancy and protocol as ratios of mean fetal dose per mean $CTDI_{vol}$.

Additionally to the measurements of Study II, phantom AP and LAT dimensions were measured from the DICOM (digital imaging and communications in medicine) images at the level of the four surface dosimeters (see Figure 5) to allow comparisons of the measured fetal doses to the SSDEs. The effective diameters were calculated as the square root of the product of the AP and LAT dimensions, and the SSDEs were calculated based on the effective diameters (32 cm PMMA phantom) using the method described in (AAPM 2011).

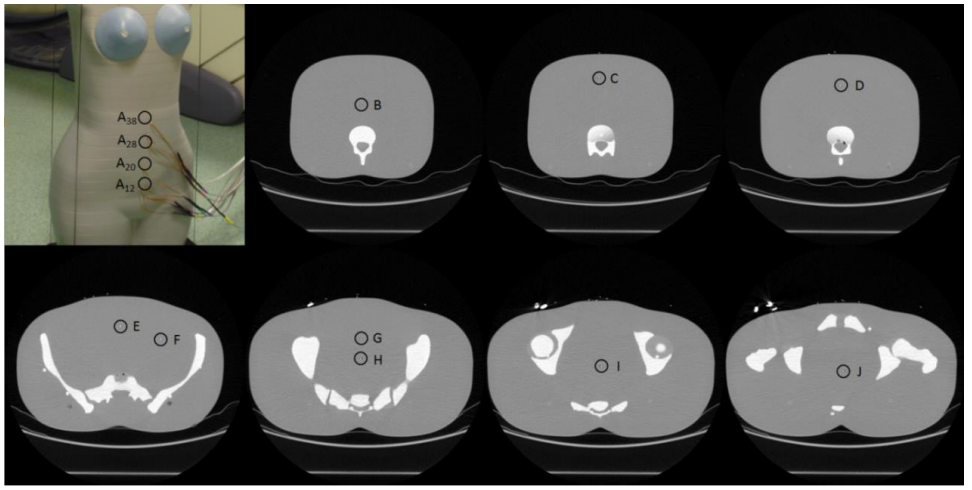

Figure 5 *MOSFET dosimeter positions A-J inside CIRS ATOM 702-D phantom in Study II.*

3.3. Mammography

In Study III, semi-circular PMMA phantoms (diameter 16 cm, thicknesses of 5 to 100 mm) (Figure 6) were exposed with full AEC (automatic exposure control) mode. Clinical settings were used in the exposures by two mammographic devices, diagnostic device Senographe Essential (GE Healthcare, Milwaukee, Wisconsin, USA) and screening device Nuance (Planmed, Helsinki, Finland), which are referred to as D1 and S1 in this thesis, respectively (Table 1). For devices D2–D8 and S2–S3 (Table 1), phantom MGD was determined during inspections performed by STUK personnel for a PMMA phantom of 45 mm thickness.

Table 1 *The mammographic devices examined in Study III by extensive phantom measurements and patient data collections (devices D1 and S1). For other devices (D2-D8 and S2-S3), phantom measurements were performed by STUK inspectors and patient data was collected by hospital staff. (Study III)*

Symbol	Manufacturer	Model	Applied anode/filter
D1	GE Healthcare	Senographe Essential	Mo/30 µm Mo Mo/25 µm Rh Rh/25 µm Rh
D2	GE Healthcare	Performa	Mo/30 µm Mo
D3	Planmed	Nuance Excel	W/75 µm Ag
D4	Planmed	Nuance Classic	Mo/30 µm Mo
D5	Siemens	Mammomat Inspiration	W/50 µm Rh
D6	Siemens	Mammomat Inspiration	W/50 µm Rh
D7	Siemens	Mammomat Inspiration	W/50 µm Rh
D8	Siemens	Mammomat 3000 NOVA	Mo/30 µm Mo
S1	Planmed	Nuance	W/60 µm Rh W/75 µm Ag
S2	GE Healthcare	Alpha Performa	Mo/30 µm Mo
S3	Planmed	Nuance Excel	W/75 µm Ag

D = Diagnostic device, S = Screening device

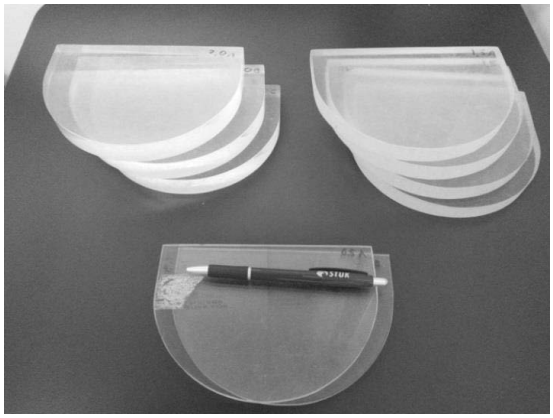

Figure 6 *Mammography PMMA phantoms from STUK, Helsinki, Finland used in Study III.*

In Study III, dose measurements were performed according to national mammography dose protocol (Toroi et al. 2011; Toroi et al. 2013). K_a was measured with an ionisation chamber of type 10×5^{-6} M (Radcal Corporation). Y(d) was calculated according to Equation (5). HVL was measured by adding additional Al filtration layers on the compression paddle and measuring the Al thickness that was needed to halve the K_a. MGDs were calculated according to Equation (11).

In Study III, patient data were collected for CC and MLO projections (see Figure 7) so that surgically operated breasts and breast implants were excluded from the collection. For devices D2–D8 and S2–S3, patient data were collected by hospital staff for a minimum of ten patients with breast thicknesses in the range of 40–60 mm, with an average of 50 mm. For D1, DoseWatch software (GE Healthcare, Milwaukee, Wisconsin, USA) was used in diagnostic patient data collection (patient age interval 22–97 years, time interval 195 days), and MGDs for 5342 exposures were determined. For S1, exposure parameters and CBTs from 100 screening examinations (patient age interval 50–69 years) were manually collected by hospital staff and MGDs for 395 exposures were determined.

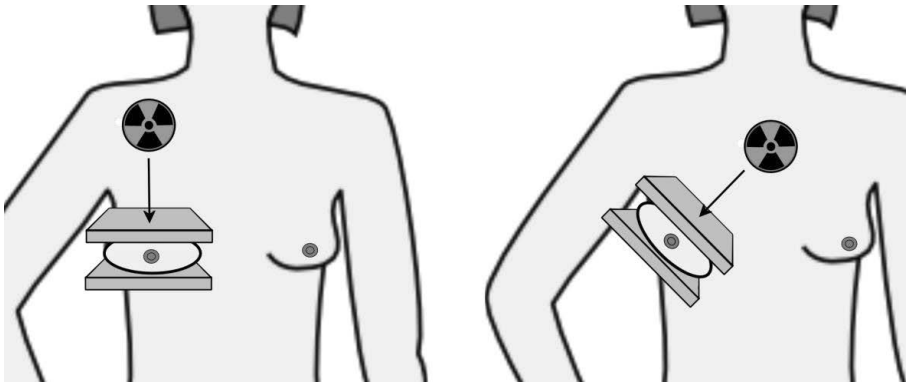

Figure 7 *Patient data was collected in Study III for the standard projections used in mammography: right craniocaudal (CC, left image) and right mediolateral oblique (MLO, right image).*

3.4. Dental radiography

In Study IV, the doses were measured as air kerma with a RaySafe Xi unit using 8202062-C Xi Survey Detector (Unfors RaySafe AB, Billdal, Sweden) inside an anthropomorphic adult female phantom (CIRS ATOM 702-D, Norfolk, USA) at the slice 21 position, which was removed and replaced with wooden spacers as separators to provide a gap for the dose measurement (Figure 8). This position represented the liver level and the apex of the fetal coverage in late pregnancy. Doses were also measured at the breast level outside the phantom by attaching the detector between the breasts. The average doses at the measurement positions were used as the upper estimates for the fetal and breast doses. Fetal and breast dose conversion coefficients were calculated as the average dose divided by the DAP value of the examination.

Figure 8 *CIRS ATOM 702-D phantom and wooden spacers in Study IV.*

In Study IV, four dental modalities were used: intraoral, panoramic, cephalometric and CBCT. The tube output of the intraoral round cone device (Planmeca ProX, Planmeca, Helsinki, Finland) was measured with a RaySafe Xi unit using an 8202031-J Xi R/F & MAM detector (Unfors RaySafe AB, Billdal, Sweden). The projections in the Planmeca ProX intraoral round cone device were upper occlusal from a +65° vertical angle, which served as the worst case scenario for the fetus, mandibular incisor from a -5° vertical angle and right maxillary premolar from a +17° vertical angle. A Planmeca Pro Max 2D S2 was used in panoramic examinations and a Planmeca ProMax cephalostat was used in lateral cephalometric examinations. A Planmeca ProMax 3D Mid (Planmeca) was used in CBCT examinations with small, medium, large and extra large fields of view (FOVs). The exposure parameters used in all dental modalities examined in Study IV were those recommended by the device manufacturer (Planmeca).

Doses were measured both with and without lead shielding in Study IV. The lead shields used were lead shield for thyroid only (Shield 1, 0.5 mmPb, model RA 615, MAVIG), lead shield for thyroid, breasts and abdominopelvic region (Shield 2, 0.5 mmPb, model RD 642-

99, MAVIG) and lead apron for breasts and upper abdomen (Shield 3, 0.5 mmPb, model 642, MAVIG). Shields 1 and 2 were used in the intraoral modality, and Shield 3 in the other modalities according to clinical practice.

4. Results

Table 2 shows the organs of interest, radiation type (direct or scattered radiation), use of shielding and the focuses of each study, which are related to the aims of this thesis.

Table 2 *The studies I-IV included in this thesis. Numbers on parenthesis refer to the aims 1.-4. of the study.*

Study	Modality	Organ	Direct beam/scattered radiation	Shielding	Focus (aim number)
I	General radiography	Breasts, lungs	Direct + scatter	No	PCXMC phantom versus patients (1) Effect of radiation quality and patient size (3)
II	CT	Fetus	Direct + scatter	No	Conv. coefficients from $CTDI_{vol}$ to fetal dose (2) Effect of patient size (3)
III	Mammography	Glandular tissue of the breast	Direct	No	PMMA phantom versus patient (1) Effect of radiation quality and patient size (3)
IV	Dental radiography	Fetus, breasts	Scatter	Yes	Conv. coefficients from DAP to fetal and breast dose (2) Effect of lead shields (4)

4.1. Comparison of doses to phantoms with doses to patients

In Study I, the ImpactMC results for lungs were up to 16% lower than the PCXMC results at the same patient AP thickness. For patients with small AP thickness, the ImpactMC results for breasts were up to 52% higher than the PCXMC results, and for patients with large AP thickness, the ImpactMC results were up to 55% lower than the PCXMC results. AP thickness of 208 mm (female XS) refers to small patients and AP thickness of 269 mm (female XL) for large patients, respectively. The results are shown in Figure 9 and Table 6.

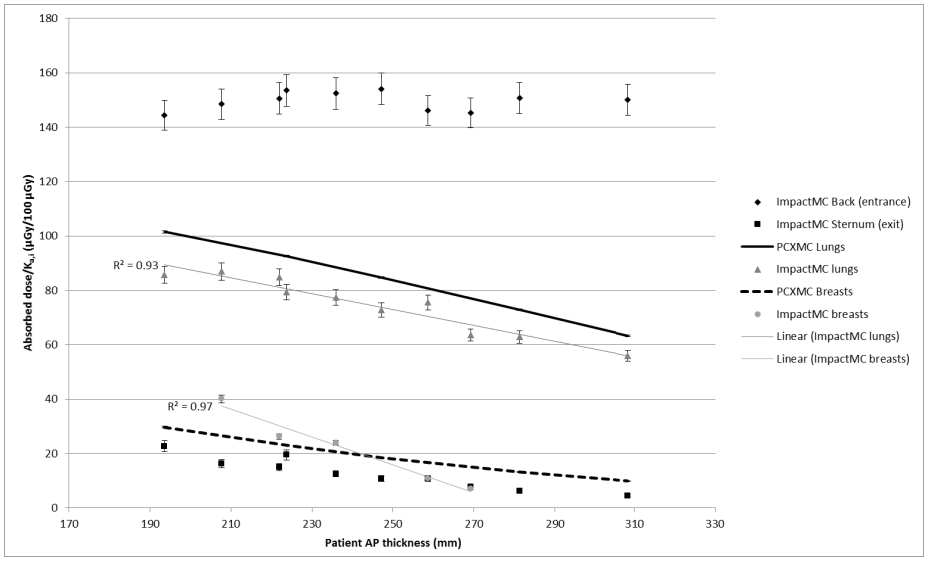

Figure 9 *Comparison of Monte Carlo simulation based organ dose conversion coefficients for lungs and breasts for different anterior-posterior (AP) thicknesses at the reference radiation quality (120 kV and 4 mmAl + 0.2 mmCu.) (Study I)*

According to Study III, the difference between the phantom ($MGD_{ph,c}$) and patient ($MGD_{pa,c}$) MGD curves calculated with glandularity correction varied from 0 to 25% and from 0 to 20% depending on thickness for diagnostic device 1 (D1) and screening device 1 (S1), respectively. In the thickness range of 40–60 mm, the maximum difference between phantom and patient curves was 26% and less than 5% for D1 and S1, respectively. The patient and phantom MGD curves of Study III are shown in Figures 10 and 11.

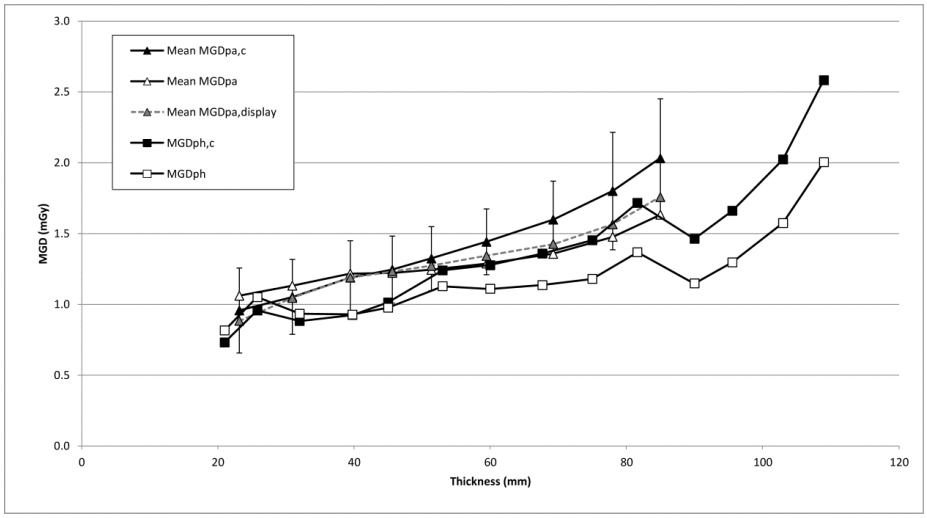

Figure 10 *Patient and phantom MGDs for diagnostic device 1 (D1) as a function of the equivalent breast thickness. Patient mean MGDs calculated with (MGDpa,c, black triangles) and without (MGDpa, white triangles) glandularity correction are presented with SDs. Mean display values (MGDpa,display, grey triangles) are shown for patients. Phantom MGDs calculated with (MGDph,c, black squares) and without (MGDph, white squares) glandularity correction. (Study III)*

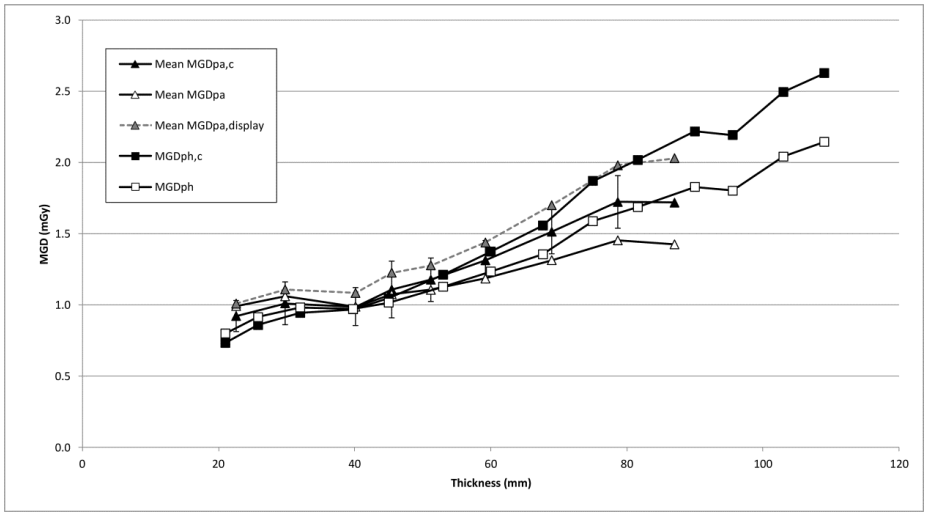

Figure 11 *Patient and phantom MGDs for screening device 1 (S1) as a function of the equivalent breast thickness. Patient mean MGDs calculated with (MGDpa,c, black triangles) and without (MGDpa, white triangles) glandularity correction are presented with SDs. Mean display values (MGDpa,display, grey triangles) are shown for patients. Phantom MGDs calculated with (MGDph,c, black squares) and without (MGDph, white squares) glandularity correction. (Study III)*

Comparison of MGDs in Study III determined for the standard phantom (MGDph (45 mm)) and patients in the CBT range of 40 to 60 mm with an average of 50 mm (mean MGDpa (50 mm)) for the devices D1–D8 and S1–S3 (Table 1) is shown in Figure 12. For devices D1 and S1, the values calculated without glandularity correction (c = 1) are shown. The DLR for MGD in Finland is 1.5 mGy, which is also shown in Figure 12. The difference between MGDph (45 mm) and mean MGDpa (50 mm) values was up to 30%, compared to MGDph (45 mm).

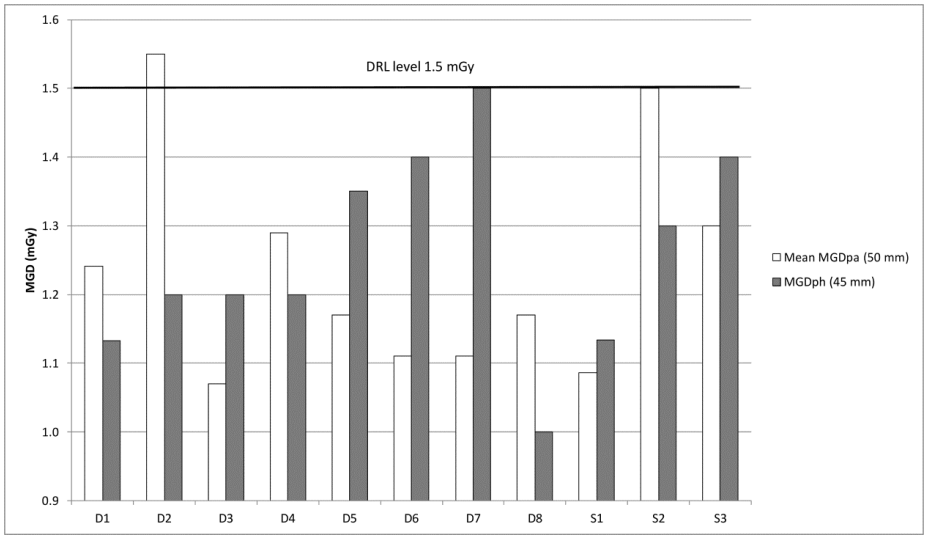

Figure 12 *Standard phantom MGDs (MGDph (45 mm)), and patient mean MGDs (MGDpa (50 mm)) for devices D1–D8 and S1–S3. For D1 and S1, the values calculated without glandularity correction (c =1) are shown. (Study III)*

4.2. Conversion coefficients for fetal dose estimation

According to Study II, the relative mean fetal doses for trauma protocol in different stages of pregnancy (12, 20, 28 and 38 weeks) were in the range of 0.80–0.97 relative to the mean $CTDI_{vol}$. For abdominopelvic protocol, the relative mean fetal dose was 0.57–0.79 and for pulmonary angiography protocol, 0.01–0.05 relative to the mean $CTDI_{vol}$, respectively. These relative fetal doses can be used as conversion coefficients in fetal dose estimation in different stages of pregnancy and in different CT protocols (see Table 3). The $C_{a,c}$ reference value for these settings was 16 mGy.

In Study IV, fetal dose conversion coefficients were calculated relative to the DAP value, both with and without lead shielding for three intraoral projections and panoramic, cephalometric and CBCT examinations. Results of Study IV are shown in Tables 4 and 5.

Table 3 *The measured fetal doses (D_f, in mGy) in pregnancy stages of 12, 20, 28 and 38 weeks with the variation range in parenthesis for trauma, abdomino-pelvic and pulmonary angiography CT protocols. Relative fetal doses are calculated relative to the mean $CTDI_{vol}$ (in mGy), and serve as fetal dose conversion coefficients (in mGy/mGy). (Study II)*

Protocol	12 weeks	20 weeks	28 weeks	38 weeks
Trauma				
Mean D_f	4.60 (4.21-5.26)	4.87 (4.21-5.59)	4.39 (3.30-5.12)	4.64 (3.45-5.46)
Mean $CTDI_{vol}$	4.74	5.15	5.30	5.79
Relative dose	0.97	0.95	0.83	0.80
Abdomino-pelvic				
Mean D_f	2.06 (1.83-2.51)	2.41 (1.94-3.07)	2.14 (1.62-2.61)	2.21 (1.79-2.71)
Mean $CTDI_{vol}$	2.63	3.04	3.22	3.91
Relative dose	0.78	0.79	0.66	0.57
Pulmonary angiography				
Mean D_f	0.01 (0.008-0.014)	0.03 (0.006-0.12)	0.06 (0.004-0.25)	0.09 (0.011-0.29)
Mean $CTDI_{vol}$	1.34	1.46	1.54	1.97
Relative dose	0.01	0.02	0.04	0.05

Table 4 *The measured fetal doses, lead shield dose reduction in percentages and fetal dose conversion coefficients calculated relative to the dose-area product (DAP) values in intraoral examinations (Study IV).*

	Foetal dose			**Breast dose**		
Modality	No shield	Lead thyroid shield (Shield 1)	Lead apron and thyroid shield (Shield 2)	No shield	Lead thyroid shield (Shield 1)	Lead apron and thyroid shield (Shield 2)
Intraoral (µGy)						
Upper occlusal	0.553	0.022	0.017	1.882	0.994	0.016
Dose reduction (%)		96	97		47	99
Conversion coefficient (µGy/Gycm^2)	27.0	1.1	0.8	0.0917	0.0485	0.0008
Mandibular incisor	0.009	0.006	-	0.602	0.283	0.002
Dose reduction (%)		39			53	>99
Conversion coefficient (µGy/Gycm^2)	1.0	0.6		67.7	31.8	0.3
Maxillary premolar (right)	0.012	0.005	-	0.659	0.512	0.004
Dose reduction (%)		57			22	99
Conversion coefficient (µGy/Gycm^2)	0.7	0.3		39.3	30.5	0.2

Table 5 *The measured fetal doses, lead shield dose reduction in percentages and fetal dose conversion coefficients calculated relative to the dose-area product (DAP) values in panoramic, cephalometric and cone beam computed tomography (CBCT) examinations (Study IV).*

	Foetal dose		**Breast dose**	
	No shield	Lead apron (shield 3)	No shield	Lead apron (shield 3)
Panoramic dose (µGy)	0.11	0.04	3.57	0.61
Dose reduction (%)		61		83
Conversion coefficient (µGy/Gycm^2)	1.5	0.6	50.3	8.6
Cephalometric dose (µGy)	0.71	0.69	4.33	0.08
Dose reduction (%)		3		98
Conversion coefficient (µGy/Gycm^2)	44.4	43.1	270.8	5.2
CBCT dose (µGy)				
Small FOV	2.64	0.80	43.20	5.74
Dose reduction (%)		70		87
Conversion coefficient (µGy/Gycm^2)	4.7	1.4	77.6	10.3
Medium FOV	3.75	1.10	61.90	9.09
Dose reduction (%)		71		85
Conversion coefficient (µGy/Gycm^2)	4.6	1.3	75.5	11.1
Large FOV	4.52	1.28	75.26	10.36
Dose reduction (%)		72		86
Conversion coefficient (µGy/Gycm^2)	4.1	1.2	68.9	9.5
Extra-large FOV	6.93	2.11	75.38	8.24
Dose reduction (%)		69		89
Conversion coefficient (µGy/Gycm^2)	2.8	0.8	30.3	3.3

FOV = field of view

4.3. The effect of patient size on organ doses

In Study I, the highest variations relative to the mean and reference values were found in ImpactMC results for breasts (Table 6). For patients with small AP thickness, organ doses are up to 5.7 times larger than for patients with large AP thickness.

Table 6 *Monte Carlo simulation results for the different patient and phantom anterior-posterior (AP) thicknesses in thorax posterior-anterior (PA) examination, expressed as conversion coefficients calculated relative to the incident air kerma (Study I).*

Patient thickness							
		Minimum AP thickness: 194 mm	Maximum AP thickness: 308 mm	Mean	Reference[1] AP thickness: 200 mm	Variation relative to mean	reference
		Conversion coefficients (μGy/100μGy)				variation range (%)	
PCXMC	Lung	102	63	83	96	46	40
	Breast	30	10	19	27	105	73
ImpactMC	Lung	86	56	74	96	40	31
	Breast	40[2]	7[2]	22	27	153	122

[1] PCXMC phantom with standard dimensions [2] The minimum and maximum AP thicknesses for ImpactMC breast results are 208 mm and 269 mm, respectively (female extra small and extra large patients)

In Study II, the automated tube current modulation (ATCM) kept the mean fetal dose rather constant through all pregnancy stages in trauma and abdomino-pelvic protocols (Table 3). In pulmonary angiography protocol, however, the mean fetal dose increased exponentially as the distance from the end of the scan range decreased (Table 3).

In Table 7 the measured AP and LAT dimensions and the calculated effective diameters of the female phantom used in Study II are presented for the different pregnancy stages. The SSDEs were calculated based on the effective diameters and the $CTDI_{vol}$ values presented in Table 3.

Table 7 *Measured anterior-posterior (AP) and lateral (LAT) dimensions and the calculated effective diameters for Study II. Calculated size-specific dose estimates (SSDEs) and measured fetal doses are shown for the different pregnancy stages and computed tomography (CT) protocols a, b and c.*

Pregnancy stage (weeks)	**AP dimension (cm)**	**LAT dimension (cm)**	**Effective diameter (cm)**	**Calculated SSDE [(a/b/c)] (mGy)**	**Mean D_f[(a/b/c)] (mGy)**
12	20.07	33.26	25.84	6.78/3.76/1.92	4.60/2.06/0.01
20	24.43	30.66	27.37	7.06/4.16/2.00	4.87/2.41/0.03
28	25.88	24.33	25.09	7.84/4.77/2.28	4.39/2.14/0.06
38	27.56	21.23	24.19	8.86/5.98/3.01	4.64/2.21/0.09

[a] Trauma, [b] Abdomino-pelvic, [c] Pulmonary angiography, SSDE = size-specific dose estimate, D_f = fetal dose

The results of Study III showed that the average CBT was close to the nationally used reference of 50 mm in diagnostic (average CBT 50 mm, SD 13 mm) and screening (average CBT 47 mm, SD 13 mm) examinations. The average MGD for all thicknesses and both CC and MLO projections differed by less than 2 % from the MGD determined for breasts in the limited CBT range of 40–60 mm (Tables 8 and 9).

Table 8 *Compressed breast thickness (CBT) and mean glandular dose (MGD) for the diagnostic mammographic device D1. The variation ranges are shown in parenthesis. (Study III)*

	Projection	Displayed mean CBT (min-max)	Displayed mean MGD_{pa} (min-max)	Calculated mean $MGD_{pa,c}$ (min-max)	Calculated mean MGD_{pa} (min-max)
Unit		mm	mGy	mGy	mGy
All thicknesses	CC, MLO	50.3 (16.0–119.0)	1.26 (0.47–7.20)	1.33 (0.48–6.09)	1.25 (0.41–4.83)
40-60 mm	CC, MLO	49.8	1.26 (0.68–2.19)	1.31 (0.70–2.22)	1.24 (0.62–2.17)
All thicknesses	CC	47.4 (16.0–86.0)	1.19 (0.57–3.43)	1.24 (0.62–4.02)	1.19 (0.65–3.41)
40-60 mm	CC	49.5	1.22 (0.71–2.19)	1.26 (0.70–2.22)	1.20 (0.68–2.17)
All thicknesses	MLO	53.0 (19.0–119.0)	1.34 (0.47–7.20)	1.41 (0.48–6.09)	1.31(0.41–4.83)
40-60 mm	MLO	50.2	1.31 (0.68–2.11)	1.35 (0.72–2.11)	1.28 (0.62–2.15)

CC = craniocaudal, MLO = mediolateral oblique

Table 9 *Compressed breast thickness (CBT) and mean glandular dose (MGD) for the screening mammographic device S1. The variation ranges are shown in parenthesis. (Study III)*

	Projection	Displayed mean CBT (min-max)	Displayed mean MGD_{pa} (min-max)	Calculated mean $MGD_{pa,c}$ (min-max)	Calculated mean MGD_{pa} (min-max)
Unit		mm	mGy	mGy	mGy
All thicknesses	CC, MLO	47.0 (15.0–87.0)	1.27 (0.69–2.29)	1.15 (0.66–1.99)	1.10 (0.71–1.79)
40-60 mm	CC, MLO	48.8	1.25 (0.92–2.02)	1.14 (0.84–1.83)	1.09 (0.84–1.79)
All thicknesses	CC	45.2 (17.0–78.0)	1.21 (0.74–1.99)	1.10 (0.68–1.79)	1.06 (0.75 – 1.58)
40-60 mm	CC	48.2	1.22 (0.93–1.78)	1.11 (0.86–1.62)	1.06 (0.84 – 1.56)
All thicknesses	MLO	48.8 (15.0–87.0)	1.33 (0.69–2.29)	1.20 (0.66–1.99)	1.14 (0.71 – 1.79)
40-60 mm	MLO	49.6	1.29 (0.92–2.02)	1.18 (0.84–1.83)	1.12 (0.84 – 1.79)

CC = craniocaudal, MLO = mediolateral oblique

4.4. The effect of radiation quality on organ doses

According to Study I, with the same measurable incident dose level, organ doses differ by a factor of up to 3.5 depending on the radiation quality (Table 10). Lung dose conversion coefficients are presented as a function of the tube voltage and HVL in Figures 13 and 14, respectively.

Table 10 *Monte Carlo simulation results for the different radiation qualities in thorax posterior-anterior (PA) examination, expressed as conversion coefficients calculated relative to the incident air kerma (Study I).*

Radiation quality							
		Minimum HVL: 2.6 mmAl	Maximum HVL: 8.5 mmAl	Mean	Reference[1] HVL: 8.1 mm Al	Variation relative to mean	Variation relative to reference
		Conversion coefficients (µGy/100µGy)				variation range (%)	
PCXMC	Lung	45	98	75	96	71	55
	Breast	8	28	19	27	107	74

[1]PCXMC phantom with standard dimensions.

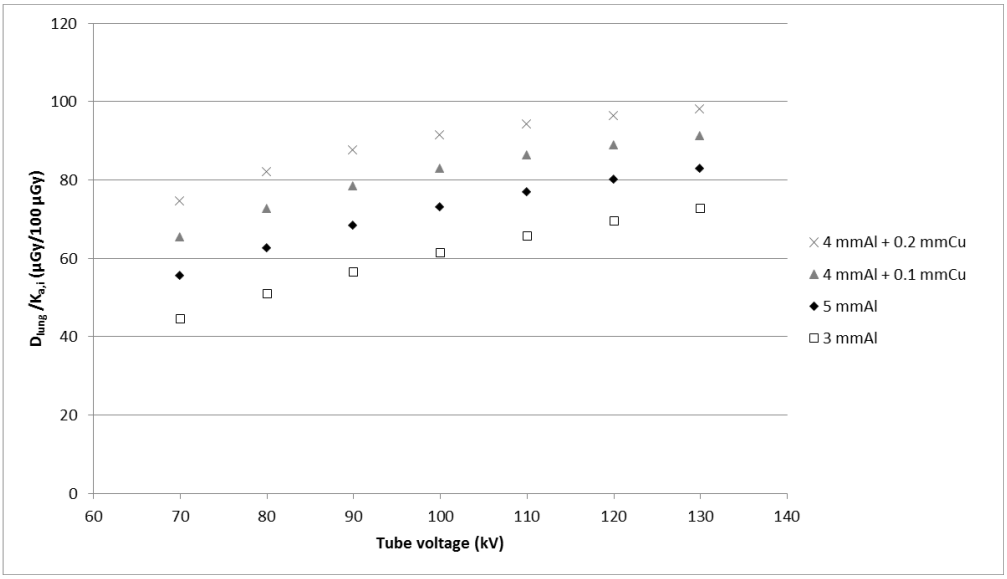

Figure 13 *Lung dose conversion coefficients relative to the incident air kerma from PCXMC simulations in thorax posterior-anterior (PA) examination for different total filtrations as a function of the tube voltage (Study I).*

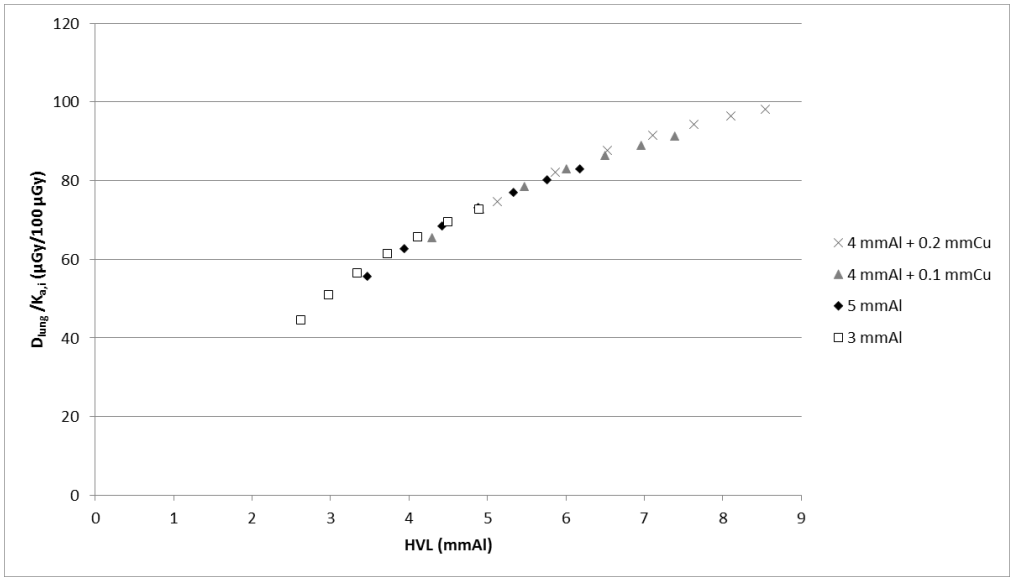

Figure 14 *Lung dose conversion coefficients relative to the incident air kerma from PCXMC simulations in thorax posterior-anterior (PA) examination for different total filtrations as a function of the half value layer (Study I).*

In Study III, the radiation qualities selected by the AEC in phantom and patient exposures varied, as can be seen from Tables 11 and 12. For S1, there were no patients with breast thickness of 68 mm exposed with the same radiation quality as the phantom with equivalent breast thickness of 68 mm. This was also the case for thicknesses of more than 68 mm, where the difference in the radiation quality was even larger (Table 12). Non-linearities in the phantom data of D1 shown in Figure 10 are due to radiation quality changes (anode, filter and tube voltage) as a function of CBT. In Figure 11 this kind of behaviour is not seen for S1, because the radiation quality changes are mainly tube voltage changes, and the filter is changed only for very small CBTs (Tables 11 and 12).

Table 11 *PMMA phantom thicknesses and the related equivalent breast thicknesses, mean patient compressed breast thicknesses (CBTs) with ranges in parenthesis, calculated phantom and mean patient glandular doses (MGDs) with ranges in parenthesis and radiation qualities from phantom and patient exposures for the diagnostic mammographic device D1 (Study III).*

Phantom thickness (mm)	Equivalent breast thickness (mm) (Dance et al. 2000)	Phantom $MGD_{ph,c}$ (mGy)	Phantom MGD_{ph} (mGy)	Radiation quality from phantom exposure (anode/filter/kV)	Mean CBT (mm) (range)	Mean patient $MGD_{pa,c}$ (mGy) (min-max)	Radiation qualities in patient studies (anode/filter/kV)
20	21	0.73	0.81	Mo/Mo/26	23 (0-25) n=61	0.95 (0.50-2.00)	Mo/Mo/25,26; Mo/Rh/26,27; Rh/Rh/29
30	32	0.88	0.93	Mo/Rh/26	31 (25-35) n=753	1.05 (0.62-2.07)	Mo/Mo/25,26; Mo/Rh/26,27; Rh/Rh/29
35	40	0.92	0.93	Mo/Rh/27	39 (35-42.5) n=1027	1.19 (0.64-2.74)	Mo/Rh/26,27; Rh/Rh/29,30,31
40	45	1.01	0.97	Rh/Rh/29	46 (42.5-47.5) n=885	1.24 (0.70-2.17)	Mo/Rh/26,27; Rh/Rh/29,30,31
45	53	1.24	1.13	Rh/Rh/29	51 (47.5-55) n=1214	1.32 (0.74-2.22)	Mo/Rh/27; Rh/Rh/29,30,31
50	60	1.27	1.11	Rh/Rh/29	59 (55-65) n=1230	1.44 (0.48-2.29)	Mo/Rh/26,27; Rh/Rh/29,30,31
55	68	1.36	1.13	Rh/Rh/30	69 (65-75) n=591	1.60 (0.71-2.90)	Mo/Rh/27; Rh/Rh/29,30,31
60	75	1.45	1.18	Rh/Rh/31	78 (75-82.5) n=156	1.80 (1.21-4.16)	Rh/Rh/30,31
65	82	1.71	1.37	Rh/Rh/31	85 (82.5-87.5) n=45	2.03 (1.31-2.96)	Rh/Rh/30,31
70	90	1.46	1.15	Rh/Rh/30			
80	103	2.02	1.57	Rh/Rh/30			
85	109	2.58	2.00	Rh/Rh/30			

Table 12 *PMMA phantom thicknesses and the related equivalent breast thicknesses, mean patient compressed breast thicknesses (CBTs) with ranges in parenthesis, calculated phantom and mean patient glandular doses (MGDs) with ranges in parenthesis and radiation qualities from phantom and patient exposures for the screening mammographic device S1 (Study III).*

Phantom thickness (mm)	Equivalent breast thickness (mm) (Dance et al. 2000)	Phantom $MGD_{ph,c}$ (mGy)	Phantom MGD_{ph} (mGy)	Radiation quality from phantom exposure (anode/filter/kV)	Mean CBT range (mm) (range)	Mean patient $MGD_{pa,c}$ (mGy) (min-max)	Radiation qualities in patient studies (anode/filter/kV)
20	21	0.73	0.80	W/Rh/29	23 (0-25) n=36	0.92 (0.66-1.07)	W/Rh/29; W/Ag/30
30	32	0.94	0.98	W/Ag/30	30 (25-35) n=45	1.01 (0.81-1.52)	W/Ag/30
35	40	0.97	0.97	W/Ag/30	40 (35-42.5) n=91	0.99 (0.81-1.65)	W/Ag/30
40	45	1.04	1.02	W/Ag/30	45 (42.5-47.5) n=75	1.11 (0.86-1.83)	W/Ag/28,29,30
45	53	1.21	1.13	W/Ag/30	51 (47.5-55) n=77	1.18 (0.94-1.62)	W/Ag/28,29,30,31
50	60	1.37	1.23	W/Ag/30	59 (55-65) n=94	1.31(0.84-1.79)	W/Ag/30,31,32
55	68	1.56	1.36	W/Ag/31	69 (65-75) n=23	1.51 (1.36-1.98)	W/Ag/32,33
60	75	1.87	1.59	W/Ag/31			
65	82	2.02	1.69	W/Ag/32	79 (75-82.5) n=6	1.72 (1.58-1.99)	W/Ag/33
70	90	2.22	1.83	W/Ag/32	87 (82.5-87.5) n=1	1.72	W/Ag/34
80	103	2.50	2.04	W/Ag/33			
85	109	2.63	2.14	W/Ag/34			

4.5. The effect of lead shields on organ doses

In Study IV, the effect of the lead shields is presented as the relative dose reduction compared with the non-shielded case (Tables 3 and 4). According to Study IV, the use of lead shields reduced the fetal dose by 39–97% and the breast dose by 22%–99%, respectively. In Study IV, the upper estimates of fetal doses without and with lead shielding varied from 0.009 to 6.9 μGy and from 0.005 to 2.1 μGy, respectively. The fetal doses without and with lead shielding were far below the level associated with any practical radiation detriment to the fetus. The absolute fetal dose levels were considered negligible even without lead shielding.

5. Discussion

5.1. Phantoms versus patients in organ dose determination

In X-ray imaging, an anthropomorphic phantom is a model of the human anatomy and its X-ray attenuation and absorption properties. The construction and physical properties of different phantom types varies, and one should be aware of the conformance of phantom and patient doses. In Studies I and III, doses to standard or simplified patient models were compared with doses to patients.

In Study I, lung and breast dose conversion coefficients were determined for mathematical phantoms in PCXMC and for patients in ImpactMC based on Monte Carlo simulations. Air kerma was used as the input value for the Monte Carlo simulations, but no dose measurements were performed. Therefore, the Monte Carlo simulations of Study I are independent of dose measurements. In PCXMC, the patient model is based on a MIRD-type phantom that does not correspond to a realistic patient. However, the size of the MIRD-type phantom can be scaled by changing the phantom height and mass, but the resulting phantom thickness does not correspond to the patient thickness, when the actual height and mass of the patient are used. Therefore, the phantom mass has to be adjusted so that resulting phantom thickness equals the patient thickness. Nevertheless, the thickness-adjusted phantoms used in PCXMC do not represent the anatomical changes of different-sized patients, since the sizes of all organs and tissues are simply increased or decreased according to horizontal and vertical scaling factors. In patients, the amount of adipose tissue is usually increased in large patients, but no extra inter-organ adipose tissue is added when the patient size increases in PCXMC. The lung doses showed better conformance (differences up to 16% at the same AP thickness) than the breast doses (differences up to 55% at the same AP thickness) between phantoms and patients, as can be seen from Figure 9. The larger relative variation ranges in the ImpactMC breast results compared to the PCXMC breast results are due to larger variations in the patient anatomy than in the phantom construction. The shapes, volumes and locations of the PCXMC phantom breasts are well defined, and do not represent the considerable variations that are encountered within patients. Previously it has been found that over- or underestimations of several tens of per cent may occur for the mathematical models compared to the voxel models, and ranges of variation between different voxel models were up to 31% in lung doses and up to 84% in breast doses in the PA projection of whole body irradiations (Zankl et al. 2002).

According to Study III, determining patient MGD using only phantom measurements is inaccurate, because phantom measurements do not correspond to an extensive patient sample. The difference between 45 mm standard phantom and patient-based (CBTs 40-60 mm, average 50 mm) MGD estimations was up to 30%. Mammographic PMMA phantoms cannot simulate variations in breast composition, but they can provide standardised attenuation properties for the AEC, and are therefore appropriate to be used in addition to patient dose collections. Compared to other studies about phantom and patient MGDs (Avramova-cholakova et al. 2008; Ciraj-Bjelac et al. 2010), differences of up to 20-24% between phantom and patient MGDs have been found. However, all these differences are less than the recommended limit of 50% of the European protocol on dosimetry in mammography (European Commission 1996).

5.2. The use of conversion coefficients in fetal dose estimation

In Studies II and IV, fetal dose conversion coefficients were calculated relative to the mean $CTDI_{vol}$ (Study II) and DAP (Study IV), respectively. The rationale for providing fetal dose conversion coefficients was that they are more applicable than absolute dose values, since the fetal dose estimate can be done by multiplying the console $CTDI_{vol}$ or DAP value with the suitable conversion coefficient. In Study II, the estimated fetal dose level differs depending on the position of the fetus within the primary beam or outside of it, and in Study IV depending on the use or absence of lead shielding. The dose absorbed by the uterus has typically been used as a surrogate for the dose absorbed by the embryo and fetus in medical dosimetry (ACR 2008). As the size of the uterus increases during the pregnancy, different methods can be used to consider the larger volume compared to the non-pregnant uterus.

The results of Study II indicate that if the fetus is in the primary beam, an upper estimate of the fetal dose can be based on the $CTDI_{vol}$ console value. If the fetus is not in the primary beam, the fetal dose estimation requires considering also the distance of the fetus from the scan range. The length of the scan range and pregnancy stage should be taken into account for further evaluation of the fetal dose. The fetal dose in early pregnancy is very low, when the fetus is more than 20 cm from the caudal end of the scan range. When the fetus grows during pregnancy and the uterus extends cranially, the distance from the scan range decreases, which results in an exponential increase in the fetal dose. Compared to previous studies, it has been stated that in direct irradiation of the embryo, the embryo dose will depend on the scanned region as well as the scanned length (Huda et al. 2010). If the embryo is not directly irradiated, the embryo dose will be determined by the intensity of scattered radiation that is mainly dependent on the irradiation geometry (Doshi et al. 2008; Boone et al. 2000; Dietrich et al. 2005). However, for tissues that are 20 cm out of the beam, the dose is approximately 1% of the dose in the beam (Dietrich et al. 2005). According to Felmlee et al. (1990), the fetal dose can be estimated with an error of 15-20% based on pencil ionization chamber and TLD measurements in an anthropomorphic phantom. The largest uncertainty (25%) is related to the situation where the fetus is partially within the FOV (Damilakis et al. 2000).

The CIRS ATOM phantom (model 702-D) used in Study II represents a relatively small female (160 cm, 55 kg) and the uterus dose estimates were up to 43 % lower than the $CTDI_{vol}$ value in the abdomino-pelvic examination. According to Monte Carlo based calculations on a mathematical phantom representing a 70 kg patient, the uterus dose estimate in the abdominal or pelvic CT examinations was 40 % higher than the $CTDI_{vol}$ value (Huda et al. 2010). These differences in the uterus doses relative to the $CTDI_{vol}$ are likely to be due to the construction of the physical CIRS ATOM phantom used in Study II and the mathematical phantom used in ImPACT CT Dosimetry Calculator by Huda et al. (2010). Furthermore, when constant CT technique factors are used, embryo dose estimates for a 45 kg patient would be approximately 18 % higher than those for a 70 kg patient, whereas the corresponding embryo dose estimates for a 120 kg patient would be approximately 37 % lower (Huda et al. 2010).

It has been concluded based on MOSFET measurements in the CIRS ATOM female phantom (model 702) that fetal dose in early first trimester correlated with the $CTDI_{vol}$ via a linear regression equation in both constant tube current and ATCM modes in trauma, abdomino-pelvic and CT angiography protocols (Jaffe et al. 2008; Jaffe et al. 2009). Also a

fetal dose conversion coefficient (in mGy/mGy) for chest CT examinations of 0.02 and fetal dose conversion coefficients for abdominal CT examinations in the range of 1.01 to 1.15 have been determined based on TLD measurements in the CIRS ATOM female phantom (Helmrot et al. 2007). The fetal dose conversion coefficients during early gestation calculated based on the results of Hurwitz et al. (2006) were in line with the results of Study II for chest CT for pulmonary embolus, but higher for abdominal CT examinations. In Study II, the fetal dose normalised to $C_{a,c}$ in the abdomino- pelvic protocol in early pregnancy was in line with previously published results for GE LightSpeed VCT in early pregnancy (Damilakis, Perisinakis, et al. 2010). More recently, it has been concluded that accurate estimation of the radiation dose to the conceptus requires a patient-specific approach (Lopez-Rendon et al. 2016).

The $CTDI_{vol}$ conversion coefficients for fetal dose estimation determined in Study II were compared to other organ dose conversion coefficients. Uterus is normally a relatively average-sized organ, located in the middle of the AP dimension of the lower body. For two pediatric patients (5 weeks and 12 years old), it has been shown that $CTDI_{vol}$ underestimated dose to large organs in the scan coverage by 30% – 48% in chest and abdomino-pelvic CT examinations (Li et al. 2011b). In Study II, $CTDI_{vol}$ underestimated dose to the fetus by up to 43% in the abdomino-pelvic CT examination. Turner et al. (2011) showed that organ doses can be estimated from $CTDI_{vol}$ by multiplying $CTDI_{vol}$ by a size-dependent, scanner-independent factor. It has also been shown that in adult body CT, dose to an organ fully encompassed by the primary radiation beam can be estimated from $CTDI_{vol}$ using a protocol-independent conversion coefficient (Li et al. 2012). These kind of general conclusions cannot be drawn based on the results of Study II, because Study II was restricted to only one scanner and the special case of pregnancy.

In Studies II and IV, the conversion coefficients were based on dose measurements only. Recently it has been shown that the difference between organ doses normalized to $CTDI_{vol}$ from TLD measurements and Monte Carlo simulations on a 5 year old pediatric CIRS ATOM 705-D phantom was within ±20% for most organs, except for the bone marrow, breasts and ovaries (Dabin et al. 2016). Measured normalized organ doses were compared with those simulated using a tool that provides organ dose estimates for the ICRP reference phantoms (Lee et al. 2015). Furthermore, based on measurements on 5 different scanner models from the 4 major manufacturers, Dabin et al. (2016) stated that organ doses calculated for one CT scanner can be used to assess organ doses from other CT scanners with 20% uncertainty ($k = 1$).

In Study IV, fetal dose conversion coefficients in terms of the DAP value were calculated for situations with and without lead shielding. Previously published results on uterus doses with and without lead shielding are reviewed in Study IV, but the corresponding DAP values are not given in the studies included in the review. Therefore the comparison is done based on the absolute doses. In Study IV, the fetal dose measurements were performed the liver level, and thus providing the upper estimate of the fetal dose. Three previous studies (Buch et al. 2009; Okano et al. 2009; Okano et al. 2012) include dose measurement in the normal uterus at one to three measurement points. Consequently, the doses measured at those points should be much less than the upper estimates of the fetal dose in Study IV. However, the fetal doses measured in Study IV were smaller than the doses measured by Buch et al. (2009) in intraoral and panoramic examinations, but larger than those measured in CBCT (Okano et al. 2009; Okano et al. 2012). Since the DAP value has been suggested and used as the

DRL quantity in dental radiography (Han et al. 2012), it should be the appropriate quantity to be used in conversion coefficients.

5.3. Patient size in organ dose determination

The effect of patient size in organ dose determination was determined for lung and breast doses (Study I), fetal doses (Study II) and mean glandular doses of the breast (Study III). In Study I, the patient AP thickness was used to determine the patient size. In Study II, the focus was on different pregnancy stages and the resulting change in the morphology and habitus of the constant-sized phantom, and in Study III, only breasts of different CBTs were examined, but the size or thickness of the patient was not studied.

If patient size is not considered in the choice of the lung dose conversion coefficient, relative errors of up to 34% for the PA projection in interventional fluoroscopy procedures can be encountered (Johnson et al. 2009). Moreover, it has been found that the organ dose to an underweight patient is underestimated and the organ dose to an overweight patient overestimated if patient size is not considered when choosing a dose conversion coefficient (Johnson et al. 2009). The variation in lung doses between large patients (100 kg in mass and 170 cm in height) and an average adult has been reported to be 27% in thorax PA examinations, and that the body weight or height alone is a poor parameter for lung dose estimation (Tung et al. 2008). The body mass index (BMI) should be used instead, because the BMI is approximately linearly proportional to the patient trunk thickness (Tung et al. 2008).

As discussed earlier in chapter 5.1., when the size of mathematical phantoms is increased, it does not modify the construction of the phantom by addition of inter-organ adipose tissue, contrary to large patients, who tend to have larger amount of adipose tissue than smaller patients. Furthermore, the breasts of hermaphrodite mathematical phantoms are more fixed and they are located symmetrically in the anterior side of the phantom, whereas for patients, the size and position of breasts varies substantially. In Study I, the patient thickness had a larger relative effect on the breast dose than on the lung dose due to the position of the breasts at the patient exit and to the position of the lungs entirely within the primary beam. Previously it has been found that breast doses have less correlation with body size than lung or liver doses in chest AP examinations due to the position of breasts at the patient surface (Zhang et al. 2014). However, it has been stated that in general, organ dose conversion coefficients decrease with increasing patient size, due to the increased shielding for most organs as the body size increases (IAEA 2007). This effect was also seen in Study I in the negative slopes of the linear fits on the ImpactMC results and from the PCXMC results as a function of the patient AP thickness (Figure 9).

On the contrary, in Study III it was seen that as the CBT increases, the MGD values increased (Figures 10 and 11). This is due to the AEC that selects an appropriate radiation quality based on the pre-exposure: larger breasts require higher tube voltages and different anode/filter combinations than smaller breasts. Dance et al. (2000) have studied the average breast composition as a function of CBT. The breast has a mixture of adipose and glandular tissue. The percentage of glandular tissue decreases differently for age groups of 40-49 years and 50-64 years as a function of CBT (Dance et al. 2000).

When the attenuation on the anterior side of the phantom increased due to the added pregnancy boluses in Study II, the mean fetal dose remained quite constant because of the

ATCM, when the fetus was fully within the scanned volume. Previously, the fetal doses from TCM CT examinations have been found to remain quite stable in pregnancy stages of 15 and 20 weeks, but increase at week 31, both for mathematical and voxel phantom (Gu et al. 2013).

For projection radiography, patient SSDEs are not yet in general use. The SSDEs (AAPM 2011) provide guidance for patient size corrections in pediatric and adult body CT examinations. The SSDE conversion coefficients are given relative to the $CTDI_{vol}$, and the SSDE should correspond to tissue doses, not air kerma or other quantities. However, it has been stated that the SSDE allows average dose estimation at the center of a certain CT scan range, and that it cannot be used in organ dose estimation (Brink & Morin 2012). Moreover, while the SSDE is a simple way to estimate organ doses for relatively large organs located fully within the scan volume, for very small organs and organs only partially included in or located outside of the scan volume the SSDE will not provide a reasonable estimate of organ dose (Christner et al. 2012). It has been found in a study considering pediatric patients, from which the largest one was of the same mass as the CIRS ATOM phantom (model 702-D) used in Study II, the average correlation between SSDE and organs fully within the scan volume was better than ±10 % (Moore et al. 2014). Most recently, organ doses from CT have also been determined from post-mortem subjects with direct measurements (Griglock et al. 2015; Sinclair et al. 2015). These direct organ dose measurements can estimate organ doses more accurately than the calculated SSDE.

Comparison of the calculated SSDEs and measured fetal doses of Study II showed that for trauma and abdomino-pelvis protocols, where the fetus is fully within the scan volume, the SSDE values differed up to 91% and 171%, respectively, from the measured fetal doses. The SSDE values increased as a function of the pregnancy stage, but if the conversion coefficients for SSDE calculation are selected based on the AP dimension only, the resulting SSDE values are closer to the measured values and remain quite constant. When the fetus is outside of the scan volume in pulmonary angiography protocol, the SSDE does not provide a reasonable estimate of the fetal dose.

5.4. Radiation quality in organ dose determination

Study I showed that as a function of the HVL, the lung and breast dose conversion coefficients were more convergent than as a function of the tube voltage. This suggests that the tube voltage is not a good parameter for specifying the radiation quality alone; the total filtration also has to be defined. Previously it has been concluded that at least two specifying parameters out of the three (tube voltage, HVL and filtration) should be used (Toroi 2009). Compared to other previously published conversion coefficients from DAP to organ doses (Drexler et al. 1993; Theocharopoulos et al. 2002; Schultz et al. 1994; Petoussi-Henss et al. 1995), the results of Study I showed good correspondence.

In Study III, differences between radiation qualities selected by the AEC system for phantoms and patients were found. In modern digital mammographic devices, the appropriate radiation quality (anode, filter and tube voltage) and X-ray tube current time product (mAs) are selected by the AEC system based on breast composition and thickness. For small patient sample sizes, there might not be any patients exposed with the same radiation quality as the phantom, even if the breast thickness equals the equivalent breast thickness, which was the case in Study III with a sample size of 395 exposures. If the same

radiation quality is used for PMMA phantoms and breasts, the equivalent breast thicknesses given by Dance et al. (2000) seem to work reasonably. It must be noticed that the phantom measurement gives only one sample of the possible radiation qualities that can be selected by the AEC system.

In diagnostic radiology, the patient radiation doses need to be determined regularly and compared to the DRLs. The only modality that has an organ dose, namely MGD, as the DRL quantity is mammography, whereas for projection imaging, dental radiography and CT, application specific dosimetric quantities, $K_{a,e}$, P_{KA}, P_{KL} and C_{VOL} are used as DRLs. The uncertainties related to MGD determination are therefore higher than for directly measurable dosimetric quantities. The different mammographic devices do not necessarily calculate the MGD similarly, and the internal dose calculation method might not be easily traceable. Prior to 2011, the Finnish DRL quantity in mammography has been entrance surface dose (ESD), but MGD was implemented during the year 2011 for that purpose according to the international guidelines (European Commission 2006; IAEA 2007; ICRU 2005).

The digitalization in diagnostic radiology has increased the range of different radiation qualities. The absorption in tissues is dependent on the radiation energy, and the patient dose does not remain constant, even if ESD was unchanged (Toroi et al. 2011). MGD is a better dose quantity for estimating the radiation risk than ESD, which describes only the dose at the patient surface. However, the implementation of organ doses as the DRL quantities in other modalities than in mammography would not be applicable due to the fact that organ doses cannot be measured directly and the selected method for organ dose determination has a marked impact on the related uncertainty. In mammography, which is focused on the breast dose only, a simple method for MGD calculation is available and the mammographic devices also show the MGD values on the dose display. In other modalities, several organ are being irradiated and it would be impossible to provide on a display all the organ doses for different patients. However, in the future it would be possible to provide even the SSDE on the dose displays, but currently the DRLs are based on the dose quantities that are available on the dose displays or that can be directly measured based on patient exposures. Moreover, the application specific dose quantities also provide information about the overall performance of the devices.

5.5. Lead shields in radiation protection

The usefulness of lead shielding in dental X-ray examinations was examined in Study IV. Despite the relative shielding effect found in Study IV, the exposure-induced increase in the risk of breast cancer death for the pregnant patient (based on the breast dose only) (BEIR 2006; Tapiovaara & Siiskonen 2008) and the exposure-induced increase in the risk of childhood cancer death for the unborn child (Doll & Wakeford 1997) are of the same order of magnitude, 10^{-5}%. This is a very small value compared to the background risk of childhood cancer, which is 0.14% (Doll & Wakeford 1997). Based on the risk estimates, the need for fetal and breast lead shielding was considered irrelevant. Most important is that a clinically justified dental radiographic examination must never be avoided or postponed due to a pregnancy.

However, it is generally recognized that even a 10% reduction in patient dose is a worthwhile objective for optimization (IAEA 2007). According to Study IV, the maximum

fetal dose levels without lead shielding was less than 1% of the annual dose limit of 1 mSv for a member of the public. Compared to the natural background radiation dose rate and the dose rate in an airplane at normal cruising altitude, the accumulated dose within two days or a 2 hour flight would result in a radiation exposure of the same order of magnitude as the upper estimate for fetal dose in dental examinations. Therefore the maximum fetal dose levels are minimal, and even though they are further decreased when lead shield are used, the use of shielding to reduce the fetal dose could be considered irrelevant.

Compared to other publications on the relevance of lead shielding in dental radiography, it has been found in TLD measurements in a full body phantom that there was no statistically significant difference between absorbed organ doses in panoramic examinations with or without the use of lead apron shielding (Rottke et al. 2013). The opposite has been observed by Buch et al. (2009), who found that the use of a lead apron shielding in panoramic examinations significantly (72%) reduced the dose to the uterus. However, in full-mouth intraoral examinations, the dose reduction effect found by was small (7%) (Buch et al. 2009). A review article by Okano & Sur (2010) emphasized the importance of thyroid shielding especially for pediatric patients, because the thyroid gland is one of the most radiosensitive organs in the head and neck region. According to Study IV, thyroid shields are used in intraoral and cephalometric dental examinations, but not in panoramic examinations, because the shield may interfere with the primary beam. In CBCT, the need for thyroid shielding requires local evaluation. In the same review article by Okano & Sur (2010), it is further stated that the gonadal doses and doses to the embryo are not significant in dental radiography, but the use of lead aprons has been recommended on the grounds of patient reassurance (White et al. 2001; Whaites 2002).

The practices related to the use of lead shielding in dental X-ray examinations have varied, which is likely to raise unnecessary concerns within the pregnant women, who are unaware of their pregnancy at the time of the examination. When they learn about their pregnancy, they might be worried, if shielding was not used in their examination. Uniform practices in the use of shielding would serve both the dental staff and the patients. The findings of Study IV have been noticed in the media, and radiation protection training of dentists and other radiation workers is ongoing. The radiation protection legislation is going to change in near future, and it is really interesting to see, how attitudes and practices to very small doses are going to develop.

5.6. Uncertainties related to organ dose determination

In chapter 2.2 of this thesis, uncertainties related to each of the studied modalities were reviewed according to TRS 457 (IAEA 2007) and ICRU report No. 74 (ICRU 2005). In this chapter, those uncertainties are compared to the uncertainties of Studies I-IV and discussed briefly. It must be noted that the examples of uncertainty budgets presented in TRS 457 (IAEA 2007) are for different scenarios; the comparison in this chapter uses the largest values.

The international recommendation for the maximum uncertainty (referred to as the required accuracy) of dose measurements in diagnostic radiology is 7% ($k = 2$) if the value is used for the optimization of patient doses (IAEA 2007; ICRU 2005; Wagner et al. 1992). This value is related to the uncertainty of dosimetric quantities directly measured by the dosimeter and does not include contributions from sources used in conversion of the

measured quantity to tissue or organ doses (IAEA 2007). The uncertainty of the initial dose value, namely air kerma, is 2% (k = 2) measured in a dosimetry laboratory at one radiation quality. However, according to IAEA (2007), an uncertainty of 20% is acceptable in cases where the organ dose is low and for radiation survey measurements, but according to ICRU (2005), an uncertainty of 30-50% can be accepted when organ doses are low.

The dose detectors used in this thesis have been calibrated either at SSDL of STUK (ionisation chamber of type 10×5^{-6} M (Radcal Corporation)), or by the device manufacturer (RaySafe Xi unit with a CT detector, a Survey Detector and a R/F & MAM detector (Unfors RaySafe AB, Billdal, Sweden)). The calibration services for detectors in medical use are commonly provided only by the manufacturer, even though calibrations at the SSDL should be performed on a routine basis. The calibration was performed by Unfors RaySafe in April 2015. Therefore, the RaySafe Xi unit and its detectors were re-calibrated at STUK in September 2016.

Study I did not contain measurements, contrary to Studies II-IV. In Study I, the statistical uncertainty in ImpactMC simulations was estimated to be 2.0% (k = 2) at 10^9 photons. The uncertainties based on the minimum and maximum values of the mean doses for the back and sternum ROIs in repeated dose determinations were up to 3.2% (k = 2) and 9.0% (k = 2), respectively, and up to 3.0% (k = 2) for the lung and breast VOIs. The total uncertainty of dose values for the back and sternum ROIs was 3.8% (k = 2) and 9.2% (k = 2), respectively, and 3.6% (k = 2) for the VOIs in ImpactMC simulations. In PCXMC, the statistical uncertainties in organ dose values were up to 1.2% (k = 2) for breasts and up to 0.4% (k = 2) for lungs at 10^6 photons.

In Study II, the estimated type B uncertainty in a single MOSFET measurement with the applied dose level was 5% (k = 1), and the estimated combined standard uncertainty (type A and B) of a single MOSFET measurement was 7% − 11% (k = 1). Bone shadowing was considered to have no effect on the angular dependency of the dosimeters, because the dosimeters were far from bone structures. The uncertainty of the fetal dose measurement was affected mainly by the number of dosimeters within the fetal volume. Dose gradients could not be detected with the number of dosimeters used in Study II. The uncertainties of fetal dose estimations were larger in pulmonary angiography protocol as the fetus was outside the primary beam than in abdomino-pelvic and trauma protocols, where the fetus was within the primary beam. The sources of measurement uncertainties in computed tomography are related to the direct measurements (6.3%), the precision of reading (1.0%) and tube loading indication (1.0%), the precision of chamber and phantom positioning in the centre of gantry (0.3%), the uncertainties related to the phantom diameter and the depths of measurement bores (0.35%) and the uncertainty in chamber response for measurements inside the phantom (3.0%), which yield a combined standard uncertainty of 7.2% (k = 1) for C_W (IAEA 2007). This value was close to the estimated combined standard uncertainty of a single MOSFET measurement in Study II.

In Study III, the uncertainty estimation for MGD included uncertainties associated with air kerma calculations (5%), uncertainty in the g-factor tabulated by Dance et al. (2000) (10%), uncertainty in the g-factor associated with errors in HVL (2%) and CBT (1%), uncertainty in the c-factor tabulated by Dance et al. (2000) (5%) and maximum uncertainty in the s-factor tabulated by Dance et al. (2000) (4.6%). The estimated combined standard uncertainty in patient MGD estimation was therefore 13% (k = 1). The sources of measurement

uncertainties in mammography are related to the direct measurements (6.3%), the precision of reading (1.0%) and tube loading indication (1.0%), the uncertainty in measurement position (0.4%), the uncertainties related to HVL measurements (1.7%) and the uncertainty in a 45 mm PMMA phantom (1.7%) or in breast (6.4%) thickness (IAEA 2007). This yields a combined standard uncertainty of 6.9% (k = 1) for the phantom and 9.3% (k = 1) for a single patient (IAEA 2007). The estimated combined standard uncertainty in patient MGD in Study III was slightly larger than the combined standard uncertainty of 9.3%.

In Study IV, the repeatability of the measurements was used as an estimate of the measurement uncertainty. The relative variation in repeated measurements was the highest at the lowest measured dose level, 0.002 μGy, for which it was 45%. At the highest measured dose level, 75.4 μGy, it was 0.5%. The relative variation in repeated measurements was in each case lower than the relative dose reduction. The uncertainty of the measurement can also be estimated based on the SD of repeated measurements, and the minimum and maximum values of the repeated measurements. The combined standard uncertainty was therefore 24% (k = 1) at 0.002 μGy and 0.3% (k = 1) at 75.4 μGy. At k = 2, these values are close to the relative variation in repeated measurements. The sources of measurement uncertainties in dental radiography are related to the direct measurements (6.3%), the precision of reading (1.0%) and the uncertainty in measurement position (1.2%), which yield a combined standard uncertainty of 6.5% (k = 1) (IAEA 2007). The estimated combined standard uncertainties in Study IV depend on the measured dose level, being both smaller and larger than the combined standard uncertainty of 6.5%. In Study IV, the lowest measured dose level was close to the resolution of the used dose detector, which indicates a relatively large uncertainty.

5.7. Future prospects

The studies included in this thesis were mainly based on dose measurements rather than Monte Carlo simulations. The studies of this thesis form a whole, that encourages continuing research on the topics of this thesis based on Monte Carlo simulations and compare the results with the measurements. Ongoing and planned future studies are Monte Carlo studies about the effect pelvic lead shielding in thorax PA examination and CBCT examinations, iterative reconstruction in ultra-low dose chest CT and fetal doses in CT examinations, for example. For these studies, the anthropomorphic female phantom (CIRS ATOM 702-D, Norfolk, USA) used in the dose measurements of this thesis will be replaced by a hybrid voxel phantom, constructed from the CIRS female phantom and the ICRP Reference Female phantom. This approach makes it possible to add the extremities to the CIRS phantom in different positions, modify the head tilt angle and use the organ segmentation data of the ICRP Reference phantom.

The results of Study IV of this thesis have been presented by the author in various radiation protection trainings after the publication of the article in August 2015. These trainings have been targeted not only for dental students and specializing dentists, but also for other groups working in hospitals and other areas related to the use of ionizing radiation. The next training for dental students and specializing dentists is planned to be in January 2017.

6. Conclusions

There are large differences between doses to simplified patient models and patients, up to 55% in projection imaging and up to 30% in mammography, and the properties and limitations of the phantoms have to be understood when phantoms are used as patient models.

Conversion coefficients are more applicable in organ dose estimation than absolute doses, because the application specific dosimetric quantities are taken into account. In CT, the displayed $CTDI_{vol}$ value can be used as an upper estimate of the fetal dose in examinations, where the fetus is completely within the scan volume. When the fetus is outside of the scan volume, the fetal dose can be estimated by considering also the distance of the fetus from the scan range. In dental radiography, the conversion coefficients were calculated based on the measured upper estimates of the fetal dose, and the displayed DAP values can be used in fetal dose estimation with the conversion coefficients.

In projection imaging, the lung and breast doses decreased as the patient thickness increased, but in mammography, the MGDs increased as the compressed breast thickness increased. In CT, the ATCM kept the mean fetal dose quite constant in all studies stages of pregnancy, when the fetus was totally within the primary radiation beam. When the fetus was outside of the primary beam, the fetal dose increased exponentially, then the distance of the fetus from the scan range decreased. In the studied projection imaging examination, the HVL alone provides a more convergent specification of the radiation quality than the tube voltage, but for the tube voltage it is essential to define also the total filtration. In mammography, the effect of the radiation quality is emphasized when phantoms and patient are compared, because it is possible that the AEC selects different radiation qualities for patients and phantoms, even if the equivalent breast thickness was the same.

Despite the relative dose reduction achieved with lead shielding, the fetal dose levels without lead shielding and the related exposure-induced increase in the risk of childhood cancer death were minimal, and therefore the need for abdominal lead shielding was considered irrelevant. The exposure-induced increase in the breast cancer death was of the same order of magnitude as exposure-induced increase in the risk of childhood cancer death, and therefore also breast lead shielding was considered irrelevant. Most important is that a clinically justified dental radiographic examination must never be avoided or postponed due to a pregnancy.

References

AAPM, 2011. *AAPM Report 204 / TG-204: Size-Specific Dose Estimate (SSDE) in Pediatric and Adult Body CT Examinations*, College Park.

Abramoff, M., Magalhaes, P. & Ram, S., 2004. Image Processing with ImageJ. *Biophotonics International*, 11, pp.36–42.

ACR, 2008. ACR-SPR Practice Guideline for Imaging Pregnant or Potentially Pregnant Adolescents and Women With Ionizing Radiation. *Resolution 39*, (Amended 2014).

Agostinelli, S., Allison, J., Amako, K., Apostolakis, J., Araujo, H., Arce, P., Asai, M., Axen, D., Banerjee, S., Barrand, G., et al., 2003. Geant4—a simulation toolkit.

Nuclear Instruments and Methods in Physics Research Section A: Accelerators, Spectrometers, Detectors and Associated Equipment, 506(3), pp.250–303.

Allison, J., Amako, K., Apostolakis, J., Araujo, H., Dubois, P.A., Asai, M., Barrand, G., Capra, R., Chauvie, S., Chytracek, R., et al., 2006. Geant4 developments and applications. *IEEE Transactions on Nuclear Science*, 53(1), pp.270–278.

Avramova-cholakova, S., Vassileva, J., Borisova, R. & Atanasova, I., 2008. An estimate of the influence of the measurement procedure on patient and phantom doses in breast imaging. *Radiation Protection Dosimetry*, 129(1-3), pp.150–154.

Baró, J., Sempau, J., Fernández-Varea, J.M. & Salvat, F., 1995. PENELOPE: An algorithm for Monte Carlo simulation of the penetration and energy loss of electrons and positrons in matter. *Nuclear Instruments and Methods in Physics Research Section B: Beam Interactions with Materials and Atoms*, 100(1), pp.31–46.

Battistoni, G., Cerutti, F., Fassò, a., Ferrari, a., Muraro, S., Ranft, J., Roesler, S. & Sala, P.R., 2007. The FLUKA code: Description and benchmarking. *AIP Conference Proceedings*, 896(May), pp.31–49.

BEIR, 2006. *Committee to assess health risks from exposure to low levels of ionizing radiation. Health risks from exposure to low levels of ionizing radiation. BEIR VII.*, Washington, DC.

Birch, R. & Marshall, M., 1979. Computation of bremsstrahlung x-ray spectra and comparison with spectra measured with a Ge(Li) detector. *Phys. Med. Biol.*, 24, pp.505–17.

Blaszak, M. a. & Juszkat, R., 2014. Monte Carlo simulations for assessment of organ radiation doses and cancer risk in patients undergoing abdominal stent-graft implantation. *European Journal of Vascular and Endovascular Surgery*, 48(1), pp.23–28.

Boone, J.M., Cooper, V.N., Nemzek, W.R., McGahan, J.P. & Seibert, J.A., 2000. Monte Carlo assessment of computed tomography dose to tissue adjacent to the scanned volume. *Medical Physics*, 27(10), pp.2393–407.

Bostani, M., Mueller, J.W., McMillan, K., Cody, D.D., Cagnon, C.H., DeMarco, J.J. & McNitt-Gray, M.F., 2015. Accuracy of Monte Carlo simulations compared to in-vivo MDCT dosimetry. *Medical Physics*, 42(2), pp.1080–1086.

Brady, S.L. & Kaufman, R.A., 2012. Establishing a standard calibration methodology for MOSFET detectors in computed tomography dosimetry. *Medical physics*, 39(6), pp.3031–40.

Brenner, D.J., 2008. Effective dose: a flawed concept that could and should be replaced. *The British Journal of Radiology*, 81(967), pp.521–523.

Brenner, D.J., 2010. Should we be concerned about the rapid increase in CT usage? *Reviews on environmental health*, 25(1), pp.63–8.

Brenner, D.J., 2012. We can do better than effective dose for estimating or comparing low-dose radiation risks. *Annals of the ICRP*, 41(3-4), pp.124–128.

Brenner, D.J., Doll, R., Goodhead, D.T., Hall, E.J., Land, C.E., Little, J.B., Lubin, J.H., Preston, D.L., Preston, R.J., Puskin, J.S., et al., 2003. Cancer risks attributable to low doses of ionizing radiation: assessing what we really know. *Proceedings of the National Academy of Sciences of the United States of America*, 100(24), pp.13761–6.

Brenner, D.J. & Hall, E.J., 2007. Computed Tomography — An Increasing Source of Radiation Exposure. *New England Journal of Medicine*, 357(22), pp.2277–2284.

Brink, J. a & Morin, R.L., 2012. Size-specific dose estimation for CT: how should it be used and what does it mean? *Radiology*, 265(3), pp.666–8.

Buch, B., Fensham, R. & Maritz, M.P., 2009. An assessment of the relative safety of dental x-ray equipment. *SADJ : journal of the South African Dental Association = tydskrif van die Suid-Afrikaanse Tandheelkundige Vereniging*, 64(8), pp.348–350.

Cassola, V.F. & Hoff, G., 2010. Comparative study of computational dosimetry involving homogeneous phantoms and a voxel phantom in mammography : a discussion on applications in constancy tests and calculation of glandular dose in patients. , 43(6), pp.395–400.

Christner, J. a., Braun, N.N., Jacobsen, M.C., Carter, R.E., Kofler, J.M. & McCollough, C.H., 2012. Size-specific Dose Estimates for Adult Patients at CT of the Torso. *Radiology*, 265(3), pp.841–7.

Ciraj-Bjelac, O., Beciric, S., Arandjic, D., Kosutic, D. & Kovacevic, M., 2010. Mammography radiation dose: Initial results from Serbia based on mean glandular dose assessmentfor phantoms and patients. *Radiation Protection Dosimetry*, 140(1), pp.75–80.

Cristy, M., 1980. Mathematical phantoms representing children of various ages for use in estimates of internal dose. *Nureg/Cr-1159, ORNL/Nureg/TM-367*, pp.1–110.

Cristy, M. & Eckerman, K., 1987. Specific absorbed fractions of energy at various ages from internal photon sources. *Report ORNL/TM-8381/V1.*, pp.1–100.

Dabin, J., Mencarelli, A., McMillan, D., Romanyukha, A., Struelens, L. & Lee, C., 2016. Validation of calculation algorithms for organ doses in CT by measurements on a 5 year old paediatric phantom. *Physics in Medicine and Biology*, 61(11), pp.4168–4182.

Damilakis, J., Perisinakis, K., Tzedakis, A., Papadakis, A.E. & Karantanas, A., 2010. Radiation Dose to the Conceptus from Multidetector CT during Early Gestation: A Method That Allows for Variations in Maternal Body Size and Conceptus Position. *Radiology*, 257(2), pp.483–489.

Damilakis, J., Perisinakis, K., Voloudaki, a & Gourtsoyiannis, N., 2000. Estimation of fetal radiation dose from computed tomography scanning in late pregnancy: depth-dose data from routine examinations. *Investigative radiology*, 35(9), pp.527–533.

Damilakis, J., Tzedakis, A., Perisinakis, K. & Papadakis, A.E., 2010. A method of estimating conceptus doses resulting from multidetector CT examinations during all stages of gestation. *Medical physics*, 37(12), pp.6411–6420.

Dance, D.R., 1990. Monte Carlo calculation of conversion factors for the estimation of mean glandular breast dose. *Physics in medicine and biology*, 35(9), pp.1211–1219.

Dance, D.R., Skinner, C.L., Young, K.C., Beckett, J.R. & Kotre, C.J., 2000. Additional factors for the estimation of mean glandular breast dose using the UK mammography dosimetry protocol. *Physics in medicine and biology*, 45(11), pp.3225–3240.

Dance, D.R., Young, K.C. & van Engen, R.E., 2011. Estimation of mean glandular dose for breast tomosynthesis: factors for use with the UK, European and IAEA breast dosimetry protocols. *Physics in medicine and biology*, 56(2), pp.453–471.

Deak, P., van Straten, M., Shrimpton, P.C., Zankl, M. & Kalender, W.A., 2008. Validation of a Monte Carlo tool for patient-specific dose simulations in multi-slice computed tomography. *European Radiology*, 18(4), pp.759–772.

Dietrich, M.F., Miller, K.L. & King, S.H., 2005. Determination of Potential Uterine (Conceptus) Doses From Axial and Helical CT Scans. *Health Physics*, 88(suppl 1), pp.S10–S13.

Dietze, G., Harrison, J.D. & Menzeli, H.G., 2009. Effective dose: A flawed concept that could and should be replaced. Comments on a paper by D J Brenner (Br J Radiol 2008;81:521-3). *British Journal of Radiology*, 82(976), pp.348–350.

Dimbylow, P., 2006. Development of pregnant female, hybrid voxel-mathematical models and their application to the dosimetry of applied magnetic and electric fields at 50 Hz. *Physics in Medicine and Biology*, 51(10), pp.2383–2394.

Dimbylow, P., 2005. Development of the female voxel phantom, NAOMI, and its application to calculations of induced current densities and electric fields from applied low frequency magnetic and electric fields. *Physics in Medicine and Biology*, 50(6), pp.1047–1070.

Dimbylow, P.J., 1997. FDTD calculations of the whole-body averaged SAR in an anatomically realistic voxel model of the human body from 1 MHz to 1 GHz. *Physics in Medicine and Biology*, 42(3), pp.479–490.

Ding, A., Mille, M.M., Liu, T., Caracappa, P.F. & Xu, X.G., 2012. Extension of RPI-adult male and female computational phantoms to obese patients and a Monte Carlo study of the effect on CT imaging dose. *Physics in Medicine and Biology*, 57(9), pp.2441–2459.

Doll, R. & Wakeford, R., 1997. Risk of childhood cancer from fetal irradiation. *The British Journal of Radiology*, 70(830), pp.130–139.

Doshi, S.K., Negus, I.S. & Oduko, J.M., 2008. Fetal radiation dose from CT pulmonary angiography in late pregnancy: A phantom study. *British Journal of Radiology*, 81(968), pp.653–658.

Drexler, G., Panzer, W., Petoussi, N. & Zankl, M., 1993. Effective dose - how effective for patients? *Radiation and environmental biophysics*, 32(3), pp.209–19.

European Commission, 2006. European guidelines for quality assurance in breast cancer screening and diagnosis. In N. Perry, M. Broeders, C. De Wolf, S. Törnberg, & L. Von Karsa, eds. *Annals of oncology official journal of the European Society for Medical Oncology ESMO*. pp. 614–22.

European Commission, 1996. *European Protocol on Dosimetry in Mammography. EUR 16263*, Luxembourg.

European Parliament, 2014. Council Directive 2013/59/Euratom of 5 December 2013 laying down basic safety standards for protection against the dangers arising from exposure to ionising radiation, and repealing Directives 89/618/Euratom, 90/641/Euratom, 96/29/Euratom, 97/43/Euratom a. *Off J Eur Commun L13*, (December 2003), pp.1–73.

Felmlee, J.P., Gray, J.E., Leetzow, M.L. & Price, J.C., 1990. Estimated fetal radiation dose from multislice CT studies. *American Journal of Roentgenology*, 154(1), pp.185–190.

Fisher, H.L.J. & Snyder, W.S., 1967. Distribution of dose in the body from a source of gamma rays distributed uniformly in an organ. *ORNL-4168*.

Fisher, H.L.J. & Snyder, W.S., 1966. Variation of dose delivered by 137Cs as a function of body size from infancy to adulthood. *ORNL-4007*.

Fitzgerald, M., 1989. The commissioning and routine testing of mammographic x-ray systems topic group report 59. *Institute of Physical Sciences in Medicine*.

Goldberg-Stein, S., Liu, B., Hahn, P.F. & Lee, S.I., 2011. Body CT during pregnancy: Utilization trends, examination indications, and fetal radiation doses. *American Journal of Roentgenology*, 196(1), pp.146–151.

Griglock, T.M., Sinclair, L., Mench, A., Cormack, B., Bidari, S., Rill, L. & Arreola, M., 2015. Determining Organ Doses from CT with Direct Measurements in Postmortem Subjects: Part 1—Methodology and Validation. *Radiology*, 277(2), pp.463–470.

Gu, J., Bednarz, B., Caracappa, P.F. & Xu, X.G., 2009. The development, validation and application of a multi-detector CT (MDCT) scanner model for assessing organ doses to the pregnant patient and the fetus using Monte Carlo simulations. *Physics in Medicine and Biology*, 54(9), pp.2699–2717.

Gu, J., George Xu, X., Caracappa, P.F. & Liu, B., 2013. Fetal doses to pregnant patients from ct with tube current modulation calculated using monte carlo simulations and realistic phantoms. *Radiation Protection Dosimetry*, 155(1), pp.64–72.

Hall, E.J. & Brenner, D.J., 2008. Cancer risks from diagnostic radiology. *British Journal of Radiology*, 81(965), pp.362–378.

Hamada, N. & Fujimichi, Y., 2014. Classification of radiation effects for dose limitation purposes: History, current situation and future prospects. *Journal of Radiation Research*, 55(4), pp.629–640.

Han, S., Lee, B., Shin, G., Choi, J., Kim, J., Park, C., Park, H., Lee, K. & Kim, Y., 2012. Dose area product measurement for diagnostic reference levels and analysis of patient dose in dental radiography. *Radiation Protection Dosimetry*, 150(4), pp.523–531.

Hart, D., Jones, D. & Wall, B., 1994a. *Estimation of effective dose in diagnostic radiology from entrance surface dose and dose-area product measurements. Report NRPB-R262*, London: HMSO.

Hart, D., Jones, D. & Wall, B., 1994b. *Normalised organ doses for medical x-ray examinations calculated using Monte Carlo techniques. Report NRPB-SR262*, Chilton: NRPB.

Helasvuo, T., 2013. *Number of radiological examinations in Finland in 2011. Report STUK-B 161.*, Helsinki.

Helmrot, E., Pettersson, H., Sandborg, M. & Altén, J.N., 2007. Estimation of dose to the unborn child at diagnostic X-ray examinations based on data registered in RIS/PACS. *European Radiology*, 17(1), pp.205–209.

Le Heron, J., 1994. *XDOSE software*, National Radiation Laboratory. Ministry of Health, Christchurch, New Zealand.

Huda, W. & Gkanatsios, N. a, 1997. Effective dose and energy imparted in diagnostic radiology. *Medical physics*, 24(8), pp.1311–1316.

Huda, W., Randazzo, W., Tipnis, S., Frey, D.G. & Mah, E., 2010. Embryo Dose Estimates in Body CT. *American Journal of Roentgenology*, 194(4), pp.874–880.

Hurwitz, L.M., Yoshizumi, T., Reiman, R.E., Goodman, P.C., Paulson, E.K., Frush, D.P., Toncheva, G., Nguyen, G. & Barnes, L., 2006. Radiation dose to the fetus from body MDCT during early gestation. *American Journal of Roentgenology*, 186(3), pp.871–876.

IAEA, 2007. Dosimetry in Diagnostic Radiology: an Internacional Code of Practice. *Technical Report Series*, 457, pp.1–359.

IAEA, 2014. IAEA safety standards for protecting people and the environment. Radiation protection and safety of radiation sources: international basic safety standards. *General safety requirements part 3*.

ICRP, 1991. 1990 Recommendations of the International Commission on Radiological Protection. ICRP Publication 60. *Annals of the ICRP*, 21(1-3).

ICRP, 2009. Adult Reference Computational Phantoms. ICRP Publication 110. *Annals of the ICRP*, 39(2).

ICRP, 2002. Basic Anatomical and Physiological Data for Use in Radiological Protection Reference Values ICRP Publication 89. *Annals of the ICRP*, 32(3-4).

ICRP, 1992. ICRP, 1992. The Biological Basis for Dose Limitation in the Skin. ICRP Publication 59. *Annals of the ICRP*, 22(2).

ICRP, 1987. Protection of the Patient in Nuclear Medicine (and Statement from the 1987 Como Meeting of ICRP). ICRP Publication 52. *Annals of the ICRP*, 17(4).

ICRP, 1975. Report on the Task Group on Reference Man. ICRP Publication 23. *Annals of the ICRP/ICRP Publication*.

ICRP, 2007. The 2007 Recommendations of the International Commission on Radiological Protection. ICRP Publication 103. *Annals of the ICRP*, 37.

ICRU, 2005. International Commission on Radiation Units and Measurements. Patient dosimetry for x-rays used in medical imaging. ICRU Report 74. *J. ICRU*, 5, pp.1–113.

IEC, 2005. Medical diagnostic x-ray equipment – Radiation Conditions for use in the determination of characteristics. *IEC 61267*.

IMPACT, 2011. ImPACT CT Patient Dosimetry Calculator. Available at: http://www.impactscan.org.

ISO, 1992. *Quantities and Units — Part 0: General Principles. Report ISO 31-0*, Geneva.

ISO, 2009. *Quantities and units -- Part 1: General. Report ISO 80000-1*, Geneva.

Jaffe, T. a., Neville, A.M., Anderson-Evans, C., Long, S., Lowry, C., Yoshizumi, T.T. & Toncheva, G., 2009. Early first trimester fetal dose estimation method in a multivendor study of 16- and 64-MDCT scanners and low-dose imaging protocols. *American Journal of Roentgenology*, 193(4), pp.1019–1024.

Jaffe, T. a., Yoshizumi, T.T., Toncheva, G.I., Nguyen, G., Hurwitz, L.M. & Nelson, R.C., 2008. Early first-trimester fetal radiation dose estimation in 16-MDCT without and with automated tube current modulation. *American Journal of Roentgenology*, 190(4), pp.860–864.

Johnson, P., Lee, C., Johnson, K., Siragusa, D. & Bolch, W.E., 2009. The influence of patient size on dose conversion coefficients: a hybrid phantom study for adult cardiac catheterization. *Physics in medicine and biology*, 54(12), pp.3613–3629.

Kaasalainen, T., 2015. Optimizing Computer Tomography Examinations By Using Anthropomorphic Phantoms and Mosfet Dosimeters. *Report Series in Physics*, HU-P-D230, pp.1–63.

Knoll, G.F., 2000. *Radiation Detection and Measurement - 3rd ed.*, Hoboken, NJ: John Wiley & Sons.

Koivisto, J., Kiljunen, T., Wolff, J. & Kortesniemi, M., 2013. Characterization of MOSFET dosimeter angular dependence in three rotational axes measured free-In-Air and in soft-Tissue equivalent material. *Journal of Radiation Research*, 54(5), pp.943–949.

Kramer, R., Khoury, H.J. & Vieira, J.W., 2008. CALDose_X-a software tool for the assessment of organ and tissue absorbed doses, effective dose and cancer risks in diagnostic radiology. *Physics in medicine and biology*, 53(22), pp.6437–6459.

Kramer, R., Zankl, M., Williams, G. & Drexler, G., 1982. The calculation of dose from external photon exposures using reference human phantoms and Monte Carlo methods, Part I: The male (Adam) and female (Eva) adult mathematical phantoms. *GSF-Bericht S-885*.

Lee, C., Kim, K.P., Bolch, W.E., Moroz, B.E. & Folio, L., 2015. NCICT: a computational solution to estimate organ doses for pediatric and adult patients undergoing CT scans. *Journal of Radiological Protection*, 35(4), pp.891–909.

Lee, C., Kim, K.P., Long, D., Fisher, R., Tien, C., Simon, S.L., Bouville, A. & Bolch, W.E., 2011. Organ doses for reference adult male and female undergoing computed tomography estimated by Monte Carlo simulations. *Medical Physics*, 38(3), pp.1196–1206.

Lee, C., Kim, K.P., Long, D.J. & Bolch, W.E., 2012. Organ doses for reference pediatric and adolescent patients undergoing computed tomography estimated by Monte Carlo simulation. *Medical Physics*, 39(4), pp.2129–2146.

Lee, C., Lodwick, D., Hasenauer, D., Williams, J.L., Lee, C. & Bolch, W.E., 2007. Hybrid computational phantoms of the male and female newborn patient: NURBS-based whole-body models. *Physics in Medicine and Biology*, 52(12), pp.3309–3333.

Li, X., Samei, E., Segars, W.P., Sturgeon, G.M., Colsher, J.G., Toncheva, G., Yoshizumi, T.T. & Frush, D.P., 2011a. Patient-specific radiation dose and cancer risk estimation in CT: part I. development and validation of a Monte Carlo program. *Medical physics*, 38(1), pp.408–419.

Li, X., Samei, E., Segars, W.P., Sturgeon, G.M., Colsher, J.G., Toncheva, G., Yoshizumi, T.T. & Frush, D.P., 2011b. Patient-specific radiation dose and cancer risk estimation in CT: part II. Application to patients. *Medical physics*, 38(1), pp.408–419.

Li, X., Samei, E., Williams, C.H., Segars, W.P., Tward, D.J., Miller, M.I., Ratnanather, J.T., Paulson, E.K. & Frush, D.P., 2012. Effects of protocol and obesity on dose conversion factors in adult body CT. *Medical Physics*, 39(11), p.6550.

Lopez-Rendon, X., Walgraeve, M.S., Woussen, S., Dedulle, A., Zhang, G., Bosmans, H. & Zanca, F., 2016. Comparing different methods for estimating radiation dose to the

conceptus. *European Radiology*, pp.1–8.

Manninen, A., 2014. Clinical applications of radiophotoluminescence (RPL) dosimetry in evaluation of patient radiation exposure in radiology : determination of absorbed and effective dose. *Acta Univ Oul D. 1265*.

Martin, C.J., 2007. Effective dose: how should it be applied to medical exposures? *The British Journal of Radiology*, 80(956), pp.639–647.

Moore, B.M., Brady, S.L., Mirro, A.E. & Kaufman, R. a, 2014. Size-specific dose estimate (SSDE) provides a simple method to calculate organ dose for pediatric CT examinations. *Medical Physics*, 41(7), pp.071917–1–10.

Morant, J.J., Salvad́, M., Herńandez-Giŕon, I., Casanovas, R., Ortega, R. & Calzado, a., 2013. Dosimetry of a cone beam CT device for oral and maxillofacial radiology using Monte Carlo techniques and ICRP adult reference computational phantoms. *Dentomaxillofacial Radiology*, 42(3), pp.1–9.

Nagaoka, T. & Watanabe, S., 2009. Voxel-Based Variable Posture Models of Human Anatomy. *Proceedings of the IEEE*, 97(12), pp.2015–2025.

NRC, 2016. EGSnrc. Available at: http://www.nrc-cnrc.gc.ca/eng/solutions/advisory/egsnrc_index.html.

Okano, T., Harata, Y., Sugihara, Y., Sakaino, R., Tsuchida, R., Iwai, K., Seki, K. & Araki, K., 2009. Absorbed and effective doses from cone beam volumetric imaging for implant planning. *Dentomaxillofacial Radiology*, 38(2), pp.79–85.

Okano, T., Matsuo, A., Gotoh, K., Yokoi, M., Hirukawa, A., Okumura, S. & Koyama, S., 2012. Comparison of Absorbed and Effective Dose from Two Dental Cone Beam Computed Tomography Scanners. *Japanese Journal of Radiological Technology*, 68(3), pp.216–225.

Okano, T. & Sur, J., 2010. Radiation dose and protection in dentistry. *Japanese Dental Science Review*, 46(2), pp.112–121.

Pelowitz, D.B., 2008. MCNPX USER'S MANUAL. Version 2.6.0.

Petoussi-Henss, H., Panzer, W., Zankl, M. & Drexler, G., 1995. Dose-area product and body doses. *Radiat Prot Dosimetry*, 57, pp.363–366.

Petoussi-Henss, N., Zankl, M., Fill, U., Regulla, D. & Zanki, M., 2002. The GSF family of voxel phantoms. *Physics in Medicine and Biology*, 47(1), pp.89–106.

Radiology Masterclass, 2016. Chest X-ray Quality. Available at: http://radiologymasterclass.co.uk/tutorials/chest/chest_quality/chest_xray_quality_projection.html [Accessed May 13, 2016].

Ristic, G.S., 2013. Radiation dosimeters for medical use. *Conference on Medical Physics and Biomedical Engineering*, pp.59–64.

Rottke, D., Grossekettler, L., Sawada, K., Poxleitner, P. & Schulze, D., 2013. Influence of lead apron shielding on absorbed doses from panoramic radiography. *Dentomaxillofacial Radiology*, 42(10), pp.1–5.

Saltybaeva, N., Martini, K., Frauenfelder, T. & Alkadhi, H., 2016. Organ Dose and Attributable Cancer Risk in Lung Cancer Screening with Low-Dose Computed Tomography T. Behrens, ed. *PLOS ONE*, 11(5), pp.1–11.

Samei, E., Tian, X. & Segars, W.P., 2014. Determining organ dose: the holy grail.

Pediatric Radiology, 44(3), pp.460–467.

Sato, K., Noguchi, H., Emoto, Y., Koga, S. & Saito, K., 2009. Development of a Japanese Adult Female Voxel Phantom. *Journal of Nuclear Science and Technology*, 46(9), pp.907–913.

Schlattl, H., Zankl, M. & Petoussi-Henss, N., 2007. Organ dose conversion coefficients for voxel models of the reference male and female from idealized photon exposures. *Physics in Medicine and Biology*, 52(8), pp.2123–2145.

Schmidt, B. & Kalender, W., 2002. A fast voxel-based Monte Carlo method for scanner- and patient-specific dose calculations in computed tomography. *Physica Medica*, 18, pp.43–53.

Schultz, F.W., Geleijns, J. & Zoetelief, J., 1994. Calculation of dose conversion factors for posterior-anterior chest radiography of adults with a relatively high-energy X-ray spectrum. *British Journal of Radiology*, 67(800), pp.775–785.

Segars, W.P., Sturgeon, G., Mendonca, S., Grimes, J. & Tsui, B.M.W., 2010. 4D XCAT phantom for multimodality imaging research. *Medical physics*, 37(9), pp.4902–4915.

Seidenbusch, M.C. & Schneider, K., 2014. Conversion coefficients for determining organ doses in paediatric pelvis and hip joint radiography. *Pediatric Radiology*, 44(9), pp.1110–1123.

Sheng, Y., Tan, L., Jeon, J. & Xia, X., 2013. Development of a Voxel-based Chinese Reference Female Phantom from Color Photographs for Radiation Dosimetry Applications. *Health Physics*, 105(6), pp.512–521.

Sinclair, L., Griglock, T.M., Mench, A., Lamoureux, R., Cormack, B., Bidari, S., Rill, L. & Arreola, M., 2015. Determining Organ Doses from CT with Direct Measurements in Postmortem Subjects: Part 2—Correlations with Patient-specific Parameters. *Radiology*, 277(2), pp.471–476.

Snyder, W.S., Fisher, H.L.J., Ford, M.R. & Warner, G.G., 1969. Estimates of absorbed fractions for monoenergetic photon sources uniformly distributed in various organs of a heterogeneous phantom. *Journal of nuclear medicine : official publication, Society of Nuclear Medicine*, p.Suppl 3:7–52.

Snyder, W.S., Ford, M.R. & Warner, G.G., 1969. MIRD Pamphlet No. 5: Estimates of absorbed fractions for monoenergetic photon sources uniformly distributed in various organs of a heterogeneous phantom. *Journal of nuclear medicine : official publication, Society of Nuclear Medicine*, p.Suppl 3:7–52.

Speets, A.M., van der Graaf, Y., Hoes, A.W., Kalmijn, S., Sachs, A.P.E., Rutten, M.J.C.M., Gratama, J.W.C., Montauban van Swijndregt, A.D. & Mali, W.P.T.M., 2006. Chest radiography in general practice: Indications, diagnostic yield and consequences for patient management. *British Journal of General Practice*, 56(529), pp.574–578.

Stabin, M., Watson, E., Cristy, M., Ryman, J., Eckerman, K., Davis, J., Marshall, D. & Gehlen, K., 1995. Mathematical models and specific absorbed fractions of photon energy in the nonpregnant adult female and at the end of each trimester of pregnancy. *Oak Ridge, TN: ORNL; Report ORNL/TM-12907*.

Stamm, G. & Nagel, H.D., 2002. CT-Expo - Ein neuartiges programm zur dosisevaluierung in der CT. *RoFo Fortschritte auf dem Gebiet der Rontgenstrahlen*

und der Bildgebenden Verfahren, 174(12), pp.1570–1576.

Tapiovaara, M. & Siiskonen, T., 2008. *PCXMC. A Monte Carlo program for calculating patient doses in medical x-ray examinations. Report STUK-A231*, Helsinki.

Tapiovaara, M. & Tapiovaara, T., 2008. *The validation and user's manual of the Spektripaja (2.0) program. Report STUK-TR3*, Helsinki.

Theocharopoulos, N., Perisinakis, K., Damilakis, J., Varveris, H. & Gourtsoyiannis, N., 2002. Comparison of four methods for assessing patient effective dose from radiological examinations. *Medical physics*, 29(9), pp.2070–2079.

Tian, X., Li, X., Segars, W.P., Paulson, E.K., Frush, D.P. & Samei, E., 2014. Pediatric Chest and Abdominopelvic CT: Organ Dose Estimation Based on 42 Patient Models. *Radiology*, 270(2), pp.535–547.

Toroi, P., 2009. Patient exposure monitoring and radiation qualities in two-dimensional digital x-ray imaging. *STUK-A239*.

Toroi, P., Järvinen, H., Könönen, N. & Parviainen, T., 2011. *Determination of the radiation exposure of a patient in mammography. Report STUK-TR 11*, Helsinki.

Toroi, P., Kononen, N., Timonen, M. & Kortesniemi, M., 2013. Aspects of forward scattering from the compression paddle in the dosimetry of mammography. *Radiation Protection Dosimetry*, 154(4), pp.439–445.

Tung, C.J., Lee, C.J., Tsai, H.Y., Tsai, S.F. & Chen, I.J., 2008. Body size-dependent patient effective dose for diagnostic radiography. *Radiation Measurements*, 43(2-6), pp.1008–1011.

Turner, A.C., Zhang, D., Khatonabadi, M., Zankl, M., DeMarco, J.J., Cagnon, C.H., Cody, D.D., Stevens, D.M., McCollough, C.H. & McNitt-Gray, M.F., 2011. The feasibility of patient size-corrected, scanner-independent organ dose estimates for abdominal CT exams. *Medical physics*, 38(2), pp.820–9.

Tzamicha, E., Yakoumakis, E., Tsalafoutas, I. a., Dimitriadis, a., Georgiou, E., Tsapaki, V. & Chalazonitis, a., 2015. Dual-energy contrast-enhanced digital mammography: Glandular dose estimation using a Monte Carlo code and voxel phantom. *Physica Medica*, 31(7), pp.785–791.

UNSCEAR, 2008a. SOURCES AND EFFECTS OF IONIZING RADIATION. *Report to the General Assembly with Scientific Annexes*, Volume I, pp.1–24.

UNSCEAR, 2008b. SOURCES AND EFFECTS OF IONIZING RADIATION. *Report to the General Assembly with Scientific Annexes*, Volume II, pp.1–179.

Wagner, L.K., Fontenla, D.P., Kimme-Smith, C., Rothenberg, L.N., Shepard, J. & Boone, J.M., 1992. Recommendations on performance characteristics of diagnostic exposure meters: Report of AAPM Diagnostic X-Ray Imaging Task Group No. 6. *Medical Physics*, 19(1), pp.231–241.

Veit, R., Zankl, M., Petoussi, N., Mannweiler, E., Williams, G. & Drexler, G., 1989. Tomographic anthropomorphic models, Part I: Construction technique and description of models of an 8 week old baby and a 7 year old child. *GSF-Bericht No. 3/89*.

Veldkamp, W.J.H., Kroft, L.J.M. & Geleijns, J., 2009. Dose and perceived image quality in chest radiography. *European Journal of Radiology*, 72(2), pp.209–217.

Whaites, E., 2002. *Essentials of Dental Radiography and Radiology* 3rd ed., Edinburgh: Churchill Livingston.

White, S.C., Heslop, E.W., Hollender, L.G., Mosier, K. sM, Ruprecht, A., Shrout, M.K. & O Carrol, M.K., 2001. Parameters of radiologic care: An official report of the American Academy of Oral and Maxillofacial Radiology. *Oral Surgery, Oral Medicine, Oral Pathology, Oral Radiology, and Endodontics*, 91(5), pp.498–511.

X-5 Monte Carlo Team, 2003. MCNP–A General Monte Carlo N-Particle Transport Code, Version 5. *Los Alamos National Laboratory, Oak Ridge, TN*, 836.

Xu, X.G., 2014. *The Phantoms of Medical and Health Physics: Devices for Research and Development* A. L. DeWerd & M. Kissick, eds., New York, NY: Springer New York.

Xu, X.G., Chao, T.C. & Bozkurt, a, 2000. VIP-Man: an image-based whole-body adult male model constructed from color photographs of the Visible Human Project for multi-particle Monte Carlo calculations. *Health physics*, 78(5), pp.476–486.

Xu, X.G. & Eckerman, K.F. eds., 2009. *Handbook of Anatomical Models for Radiation Dosimetry*, Taylor & Francis.

Xu, X.G., Taranenko, V., Zhang, J. & Shi, C., 2007. A boundary-representation method for designing whole-body radiation dosimetry models: pregnant females at the ends of three gestational periods--RPI-P3, -P6 and -P9. *Physics in medicine and biology*, 52(23), pp.7023–7044.

Yoshizumi, T.T., Goodman, P.C., Frush, D.P., Nguyen, G., Toncheva, G., Sarder, M. & Barnes, L., 2007. Validation of metal oxide semiconductor field effect transistor technology for organ dose assessment during CT: Comparison with thermoluminescent dosimetry. *American Journal of Roentgenology*, 188(5), pp.1332–1336.

Zankl, M., Fill, U., Petoussi-Henss, N. & Regulla, D., 2002. Organ dose conversion coefficients for external photon irradiation of male and female voxel models. *Physics in medicine and biology*, 47(14), pp.2367–2385.

Zankl, M. & Wittmann, A., 2001. The adult male voxel model "Golem" segmented from whole-body CT patient data. *Radiation and Environmental Biophysics*, 40(2), pp.153–162.

Zhang, Y., Li, X., Segars, W.P. & Samei, E., 2014. Comparison of patient specific dose metrics between chest radiography, tomosynthesis, and CT for adult patients of wide ranging body habitus. *Medical Physics*, 41(2), pp.023901–1–12.

Zhang, Y., Li, X., Segars, W.P. & Samei, E., 2012. Organ doses, effective doses, and risk indices in adult CT: comparison of four types of reference phantoms across different examination protocols. *Medical physics*, 39(6), pp.3404–23.

Zubal, I.G., 1999. Computerized three-dimensional segmented human anatomy. *Medical Physics*, 21(2), pp.299–302.